AGU PUBLICATIONS

Paleoceanography

RESEARCH ARTICLE
10.1002/2017PA003089

Key Points:
- Revised interpretation of Bainbridge Lake sediment record based on long-term monitoring of the local climate and limnology
- Laminations within the sediment record may provide a record of both El Niño and La Niña events over the past 6000 years
- Marked increase in ENSO variability inferred starting around 1750–2000 calendar years B.P.

Supporting Information:
- Supporting Information S1

Correspondence to:
D. M. Thompson,
thompsod@bu.edu

Citation:
Thompson, D. M., et al. (2017), Tropical Pacific climate variability over the last 6000 years as recorded in Bainbridge Crater Lake, Galápagos, *Paleoceanography*, *32*, 903–922, doi:10.1002/2017PA003089.

Received 13 JAN 2017
Accepted 7 JUL 2017
Accepted article online 12 JUL 2017
Published online 26 AUG 2017

Tropical Pacific climate variability over the last 6000 years as recorded in Bainbridge Crater Lake, Galápagos

Diane M. Thompson[1], Jessica L. Conroy[2,3], Aaron Collins[4], Stephan R. Hlohowskyj[5], Jonathan T. Overpeck[5,6,7], Melanie Riedinger-Whitmore[8], Julia E. Cole[5,6], Mark B. Bush[4], H. Whitney[4], Timothy L. Corley[6], and Miriam Steinitz Kannan[9]

[1]Earth and Environment Department, Boston University, Boston, Massachusetts, USA, [2]Department of Geology, University of Illinois at Urbana-Champaign, Urbana, Illinois, USA, [3]Department of Plant Biology, University of Illinois at Urbana-Champaign, Urbana, Illinois, USA, [4]Department of Biology, Florida Institute of Technology, Melbourne, Florida, USA, [5]Department of Geosciences, University of Arizona, Tucson, Arizona, USA, [6]Department of Hydrology and Atmospheric Sciences, University of Arizona, Tucson, Arizona, USA, [7]Institute of the Environment, University of Arizona, Tucson, Arizona, USA, [8]Department of Biological Sciences, University of South Florida St. Petersburg, St. Petersburg, Florida, USA, [9]Department of Biological Sciences, Northern Kentucky University, Highland Heights, Kentucky, USA

Abstract Finely laminated sediments within Bainbridge Crater Lake, Galápagos, provide a record of El Niño–Southern Oscillation (ENSO) events over the Holocene. Despite the importance of this sediment record, hypotheses for how climate variability is preserved in the lake sediments have not been tested. Here we present results of long-term monitoring of the local climate and limnology and a revised interpretation of the sediment record. Brown-green, organic-rich, siliciclastic laminae reflect warm, wet conditions typical of El Niño events, whereas carbonate and gypsum precipitate during cool, dry La Niña events and persistent dry periods, respectively. Applying this new interpretation, we find that ENSO events of both phases were generally less frequent during the mid-Holocene (~6100–4000 calendar years B.P.) relative to the last ~1500 calendar years. Abundant carbonate laminations between 3500 and 3000 calendar years B.P. imply that conditions in the Galápagos region were cool and dry during this period when the tropical Pacific E-W sea surface temperature (SST) gradient likely strengthened. The frequency of El Niño and La Niña events then intensified dramatically around 1750–2000 calendar years B.P., consistent with a weaker SST gradient and an increased frequency of ENSO events in other regional records. This strong interannual variability persisted until ~700 calendar years B.P., when ENSO-related variability at the lake decreased as the SST gradient strengthened. Persistent, dry conditions then dominated between 300 and 50 calendar years B.P. (A.D. 1650–1900, ± ~100 years), whereas wetter conditions and frequent El Niño events dominated in the most recent century.

Plain Language Summary Sediments accumulating at the bottom of Bainbridge Crater Lake have provided a record of Galápagos climate and the frequency of El Niño events over the past ~6000 years. Motivated by the importance of this lake for our understanding of climate in the tropical Pacific Ocean, we have been monitoring the link between climate, lake conditions, and the physical and chemical properties of the lake sediments since 2009. Based on this long-term monitoring, we find that the Bainbridge sediment record preserves both El Niño and La Niña events. This makes Bainbridge a particularly valuable archive of past climate, as most sediment-based records typically preserve only one or the other key phase of tropical Pacific climate.

1. Introduction

Global climate patterns are strongly impacted by tropical Pacific Ocean sea surface temperatures (SSTs), particularly in response to departures associated with El Niño–Southern Oscillation (ENSO) events. However, observations and models disagree regarding recent temperature trends in the tropical Pacific [*Vecchi et al.*, 2008; *Deser et al.*, 2010a, 2010b; *Thompson et al.*, 2011; *Yeh et al.*, 2012; *DiNezio et al.*, 2013; *Stocker et al.*, 2013; *Jha et al.*, 2014; *Sandeep et al.*, 2014], and global climate models differ in their projections of tropical Pacific mean state and ENSO variance under increased greenhouse gas concentrations [*Guilyardi et al.*, 2012; *Kim and Yu*, 2012; *Watanabe et al.*, 2012; *An and Choi*, 2015]. The discrepancy is particularly

apparent among temperature records from the eastern Pacific, where local in situ SST measurements near Isla Santa Cruz, Galápagos, show no significant trend [*Trueman and d'Ozouville*, 2010; *Wolff*, 2010] and instrumental data indicate either a warming or slight cooling trend for the twentieth century over a broader region [*Vecchi et al*., 2008; *Deser et al*., 2010a]. The sign of the trend within these data sets also differs by season [*Karnauskas et al*., 2009; *Wolff*, 2010] and time period [*Liu et al*., 2005] analyzed. Understanding recent climate variability in the eastern Pacific is critical because this region is strongly affected by ENSO anomalies that affect much of the globe, and the trend in upwelling in this region may be key to understanding oceanic responses to radiative forcing [*Clement et al*., 1996; *Karnauskas et al*., 2009].

Paleoclimate records extend the instrumental record and improve our understanding of tropical climate variability under both natural and anthropogenic forcing. For example, paleoclimate reconstructions provide evidence for an intensification of ENSO variability (i.e., stronger and more frequent ENSO events) in the eastern Pacific in the late Holocene [*Moy et al*., 2002; *Riedinger et al*., 2002; *Koutavas et al*., 2006; *Conroy et al*., 2008; *Donders et al*., 2008]. Records from the central Pacific on the other hand display no significant change in ENSO variability from the middle to late Holocene [*Cobb et al*., 2013; *McGregor et al*., 2013], suggesting that ENSO's spatial pattern may have been altered by the background state and increased Northern Hemisphere summer insolation associated with the mid-Holocene orbital configuration [*Karamperidou et al*., 2015]. However, very few paleoclimate records from the tropical Pacific have a sufficiently high temporal resolution to separate interannual to decadal variability from changes in background state of the basin, while being long enough to study century-scale climate trends. Given that ENSO variability itself likely contributes to the discrepancy among observed and simulated trends in the tropical Pacific [e.g., *Solomon and Newman*, 2012; *Sandeep et al*., 2014], it is critical to separate high-frequency variability from long-term trends to assess the impact of natural and anthropogenic forcing on the tropical Pacific. High-resolution lake sediment records provide constraints on seasonal to millennial tropical climate variability, but uncertainties remain in the climatic interpretation of many of these records. Much of this uncertainty stems from a lack of modern observations with which to calibrate the lake sediment variables.

Sediments from Bainbridge Crater Lake, Galápagos (0°21′S, 90°34′W), are thought to be sensitive archives of past changes in tropical Pacific climate [*Riedinger et al*., 2002]. Bainbridge climate mirrors that of the broader Galápagos archipelago and has two distinct seasons: a warm/wet season from January to May and a cool/dry season from June to December [*Mitchell et al*., 1992; *Trueman and d'Ozouville*, 2010]. These seasons are driven by changes in upwelling [*Mitchell et al*., 1992] and precipitation associated with the strength of the southeast trade winds during the migration of the Intertropical Convergence Zone (ITCZ) between ~10°N in September and ~3°N in February–March [e.g., *Gruber*, 1972; *Waliser and Gautier*, 1993]. The SE trade winds and upwelling weaken as the ITCZ migrates south, bringing precipitation both north and south of the equator in the eastern equatorial Pacific during the boreal spring [*Gu et al*., 2005]. However, there is large interannual variability in the strength of wet season rainfall associated with the phase of the El Niño–Southern Oscillation. Heavy wet season rains occur during El Niño events when the trade winds and upwelling weaken, precipitation shifts eastward, and the ITCZ is pulled equatorward. In contrast, little rainfall occurs during normal or La Niña conditions, when the trade winds and upwelling are strong (as reviewed by *Kessler* [2006] and *Wang and Fiedler* [2006]). These anomalous El Niño-related rains are readily recorded in the well-mixed and hypersaline Bainbridge Crater Lake, located in the dry lowlands where interannual precipitation variability has a particularly pronounced impact.

Laminations preserved within the Bainbridge stratigraphy may record the frequency of moderate and strong El Niño events during the late Holocene [*Riedinger et al*., 2002]. *Riedinger et al*., [2002] proposed that rainfall (and/or influx of seawater) associated with El Niño events leads to the deposition of distinct carbonate or siliciclastic laminae, depending on event intensity. They proposed that siliciclastic laminae form from erosion of the crater walls during intense rainfall events, whereas carbonate laminae form during events of moderate intensity. Carbonate laminae were thought to form when rainfall is strong enough to promote lake stratification and carbonate precipitation but not erosion of the crater walls. In 2009, we began monitoring the local climate and limnology of Bainbridge Crater Lake to explore these hypotheses for laminae formation and to test how seasonal to interannual climate variability is recorded in the sediment record.

We present monitoring results from December 2009 to October 2012 (Figure 1), a period that covers more than two full seasonal cycles and a range of ENSO conditions. Based on SST anomalies in the eastern

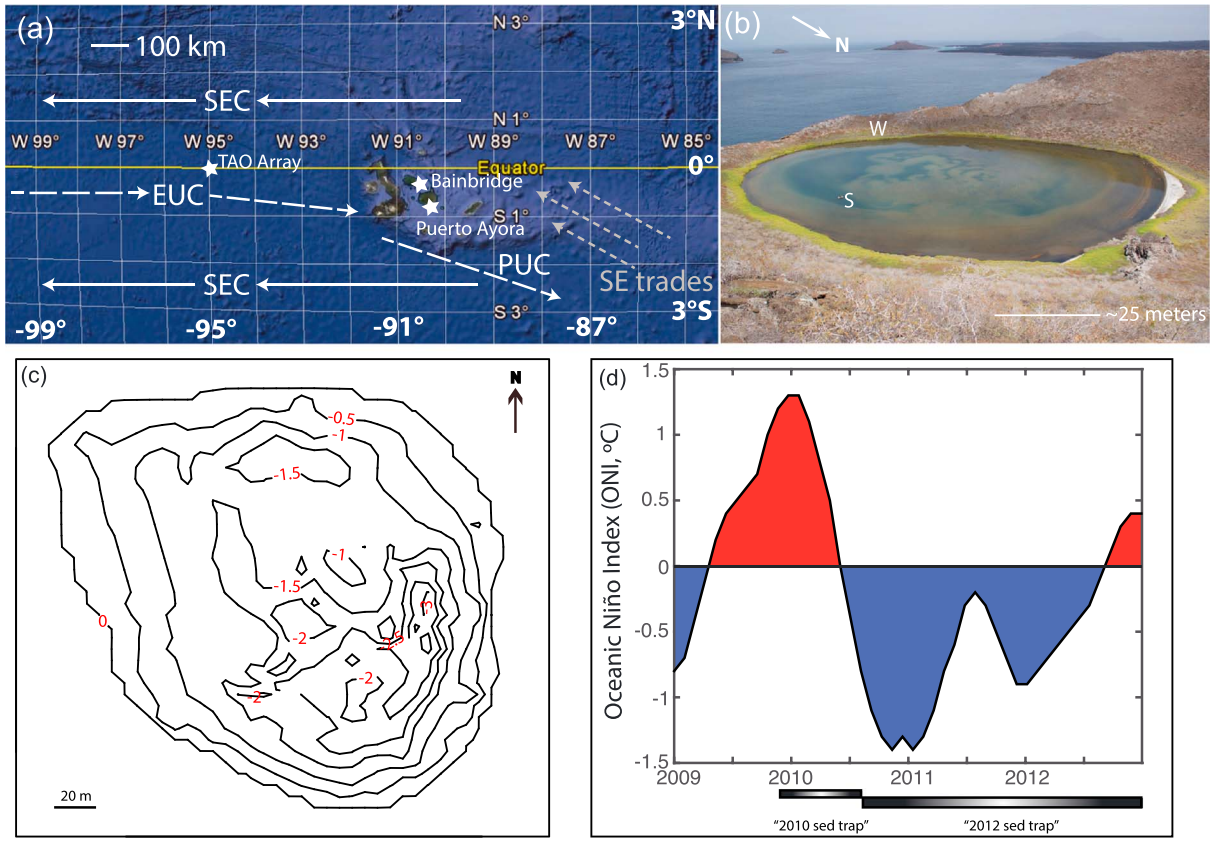

Figure 1. Geographic and temporal coverage of the Bainbridge Crater Lake monitoring data set. (a) Google Earth map (Map data: Google, Bluesky) of study region showing location of Bainbridge Crater Lake and the sites from which data were obtained for this study: meteorological stations at Bainbridge (this study) and Puerto Ayora [*Charles Darwin Foundation*, 2012] and the Tropical Atmosphere Ocean (TAO) array moored buoy at 0°N95°W. A schematic of the major surface (solid) and subsurface (dotted) currents is also included [after *Kessler*, 2006]: South Equatorial Current (SEC), Equatorial Undercurrent (EUC), Peru-Chile Undercurrent (PUC). (b) Aerial photo of Bainbridge showing the location of the weather station (W) and the deepest portion of the lake (~3.3 meters, S) where sondes and sediment traps were deployed and where sediment cores were collected in 2009 and 2012 (Photograph by S. Hlohowskyj). (c) Bathymetric map of the lake with 0.5 meter contour lines. (d) Oceanic Niño Index (ONI, °C), defined as 3 month running mean of ERSST.v4 SST anomalies in the Niño 3.4 region (5°N–5°S, 120°–170°W) [*Huang et al.*, 2015] between January 2009 and July 2012. The sediment trap monitoring periods are denoted for comparison.

tropical Pacific Niño 1 + 2 region (0–10°S, 90°W–80°W) [*Reynolds et al.*, 2002], the interval includes a weak El Niño (April 2010; daily mean Niño 1 + 2 anomaly of 0.7°C), a moderate El Niño (February–July 2012; Niño 1 + 2 = +1.4°C), and sustained La Niña conditions from July 2010 to December 2011 (Niño 1 + 2 = −1.6°C). From these monitoring results, we propose a new hypothesis for laminae formation within the Bainbridge sediment record. Applying this new climate interpretation to the sediment record, we compare our reconstruction with published reconstructions of eastern Pacific ENSO variability [*Moy et al.*, 2002; *Rein et al.*, 2005; *Conroy et al.*, 2008; *Makou et al.*, 2010] and tropical Pacific SSTs [*Koutavas et al.*, 2002; *Stott et al.*, 2004; *Rein et al.*, 2005; *Oppo et al.*, 2009] and discuss the implications for tropical climate variability over the past 6000 years.

2. Bainbridge Crater Lake

Bainbridge Crater Lake lies at sea level in the largest of the Rocas Bainbridge volcanic islands along the southeastern coast of Isla Santiago, Galápagos. The lake is small and shallow (~0.2 km in diameter and <3.3 m deep) and is nearly surrounded by moderately steep crater walls (Figure 1). The crater walls taper along the south side of the island to a low point ~2–3 m above sea level. The lake is hypersaline, with an average salinity ~3 times that of seawater (around 100 practical salinity units, psu). It is connected to the ocean through fissures in the basalt, wave action, sea spray, and storm surge over the lip of the crater wall. The vegetation on the island is dominated by the salt-tolerant *Sesuvium portulacastrum* (L.) L. and *Batis maritima* L.

plants, with *Croton scouleri* (Hook.f.) bushes lining the crater rim. American flamingos (*Phoenicopterus ruber*, Linnaeus, 1758) wade and forage in the shallow northern shore of the lake, but the sediments in the deeper sections of the lake (sampled here) are undisturbed.

3. Materials and Methods

3.1. Environmental Monitoring

3.1.1. Climate and Limnology

In December 2009, we deployed a weather station and two lake sondes to monitor the environmental conditions in and around the lake. A HOBO weather station recorded precipitation, air temperature, solar radiation, wind speed, and wind direction at 15 min intervals from 17 December 2009 to 6 June 2010 and at 30 min intervals from 6 June 2010 to 3 October 2012. To monitor the effect of local climate variability on lake conditions, we also deployed AquaTroll 100 sondes to measure temperature, electrical conductivity (EC), specific electrical conductivity, salinity, total dissolved solids, and density over the same sampling intervals. Throughout this manuscript, we report specific electrical conductivity, the electrical conductance at a standard reference temperature of 25°C, to assess changes in conductivity independent of changes in temperature of the lake and to facilitate comparison among conductivity measurements. As temperature and conductivity display a linear relationship over the monitoring period (with higher conductivity at higher temperatures), specific electrical conductivity was calculated from EC using a linear temperature compensation, with a temperature coefficient of variation at 25°C ($\alpha_{\theta,25}$) of 1.91. Continuous transects back and forth across the lake using a Garmin GPS sounding device were used to identify the deepest section of the lake and to create a bathymetric map (Figure 1c). Sondes were deployed at approximately 1 and 2 m depth on an anchor line near the deepest section of the lake (~3.1 m depth). All instruments were cleaned with freshwater and mild detergent, calibrated, and relaunched on subsequent trips in June 2010 and October 2012.

Nearly continuous daily data for the climate and limnology of Bainbridge Crater Lake were collected from December 2009 to October 2012. Daily average meteorological and limnological conditions were calculated as the average of the 15 or 30 min data between midnight and 23:45, and daily total rainfall and solar radiation were calculated as the sum over this same interval. Local meteorological data were also compared with data collected from the Charles Darwin Research Station in Puerto Ayora, Isla Santa Cruz [*Charles Darwin Foundation*, 2012] and from the nearby Tropical Atmosphere Ocean (TAO) moored buoy at 0°N, 95°W [*Hayes et al*., 1991; *McPhaden*, 1993] (Figure 1). We used the energy budget equation [after *Shanahan et al*., 2007, equation 9; *Shuttleworth*, 1993, equation 4.2.30] to calculate evaporation at the lake surface in mm/d from local air temperature, lake surface water temperature, solar radiation, and wind speed along with relative humidity from Puerto Ayora.

The first sampling period (2 December 2009 to 5 June 2010) covered one warm season and weak El Niño event, whereas the second sampling period (6 June 2010 to 2 October 2012) covered two cool seasons and two warm seasons, including an 18 month long La Niña event and a 6 month long moderate El Niño event (Figure 1). The median and distribution of daily meteorological and limnological conditions were compared between the two sediment trap sampling periods in 2010 (2 December 2009 to 5 June 2010) and 2012 (6 June 2010 to 2 October 2012), between seasons (supporting information), and among the three warm seasons (supporting information). Spearman's rank correlations were used to assess the association between the meteorological and limnological conditions at the lake. We used a linear mixed effects model to assess the relationship between meteorological and limnological conditions and sampling period and season using the lme4 package [*Bates et al*., 2015] in R [*Team*, 2014], with sampling year as a random effect to account for repeated measurements. The mixed effects model was applied to rank transform data, as this provides greater statistical power than the Friedman test for nonnormal data sets [*Zimmerman and Zumbo*, 1993; *Baguley*, 2012]. A low correlation between season and sampling period (Spearman's rank correlation; ρ = 0.35) indicates minimal impact of colinearity on these results. A likelihood ratio test (χ^2, d.f. = 1, N = 1020 for meteorological data and N = 939 for limnological data) was used to assess the impact of season and sample period, and the interaction between the two, on each climate and limnology variable.

3.1.2. Physical and Chemical Profiles

In addition to the long-term monitoring of the lake, we collected physical and chemical profiles through the water column in December 2009, June 2010, and October 2012. A hand-held YSI (Yellow Springs Instrument Company) 85 was used to collect profiles of temperature, dissolved oxygen, salinity, and conductivity, which

were also used to confirm that the sondes were deployed at depths that were representative of the lake surface and bottom. A van Dorn sampler was used to collect water samples every meter throughout the water column in the deepest portion of the lake. Water samples were collected without headspace and refrigerated until analysis. The stable oxygen isotope ratio ($\delta^{18}O$, ‰ Vienna Standard Mean Ocean Water, VSMOW) in these water samples was determined using the Thermo Delta XP plus, Gas Bench II, Isotope Ratio Mass Spectrometer at the University of Arizona (UA) ($\sigma = 0.08$). Hydrogen isotope ratios (δD, ‰ VSMOW) and replicate $\delta^{18}O$ analyses were also determined on a Finnigan Delta S gas source isotope ratio mass spectrometer in the UA Environmental Isotope Laboratory ($\sigma_{\delta 18O} = 0.08$, $\sigma_{\delta D} = 0.9$) and on a Los Gatos Research, DLT-100 (V1) instrument in the UA Department of Hydrology and Atmospheric Sciences (HAS) ($\sigma_{\delta 18O} = 0.2$, $\sigma_{\delta D} = 0.6$). Oxygen isotopic composition of the lake was compared to that of precipitation (1995–2008 average from Bellavista, Galápagos, in the Global Network of Isotopes in Precipitation, IAEA/WMO 2015) and local seawater collected during a cruise in May/June 2010. The concentrations of major and minor cations and anions were measured using an inductively coupled plasma-atomic emission spectrometer (Leeman Labs PlasmaSpec III, ±2% for major elements and ±5% for minor elements) and ion chromatography (Dionex 4000I series and AS14 column, ±1%), respectively. Alkalinity was measured by Gran-alkalinity titration [*Gieskes and Rogers*, 1973] in HAS at UA. Charge balance error (CBE) was calculated from the sum of anions (Cl, SO4, Br, and HCO3) and cations (Ca, Mg, Na, and K) following the standard method (100 × [cation − anion] / [cation + anion]) [*Freeze and Cherry*, 1979; *American Public Health Association et al*., 1998]. Finally, specific electrical conductivity (EC, mS/cm) of the water samples was measured to check for instrumental drift in the sondes deployed in the lake.

3.1.3. Basin Mineralogy and Sedimentation

To monitor lake sedimentation, sediment traps were deployed on 2 December 2009 and 6 June 2012 to collect organic and inorganic matter settling to the lake bottom. Particles were funneled into a 50 mL semitransparent polypropylene collection tube using a small plastic funnel with a collection diameter of ~10 cm (Figure S1). The openings of the sediment trap funnels were oriented vertically and deployed at 1 and 2 m depth along the sonde anchor line (~3.1 m depth). These depths were selected to avoid disturbance of the sediment traps by turbulence and resuspension at the surface and bottom of the lake. A rock mooring on the lake bottom and buoy on the lake surface kept the anchor line taught throughout the sampling period. In both collection periods, sediments overfilled the 50 mL collection tube into the overlying funnel. As a result, it was not possible to estimate the sedimentation rate from the sediment trap samples. Sediment trap samples from 2010 and 2012 were rinsed eight times with ultrapure (type 1 or Milli-Q with a resistivity of $>$18 MΩ/cm) water to remove salts and freeze dried prior to analysis. The rinsing process was performed quickly to minimize potential dissolution of gypsum in the samples.

Rock samples with varying degrees of visible weathering and a soil sample were collected from the crater rim for elemental analysis. Rock and soil samples were crushed and homogenized with a mortar and pestle prior to analysis. To map the distribution of elements in the parent rock and sediment trap samples from 2 m depth, we utilized a CAMECA SX50 electron microprobe in the Department of Planetary Sciences at the UA. Four wavelength dispersive spectrometers were run simultaneously (beam: 20 kV, 40 nA, 16 μm, and 8 ms). Samples were mounted on carbon tape and carbon coated prior to analysis. Backscattered electron images and energy dispersive spectroscopy were utilized to identify the elemental composition of the samples. An EDAX Eagle III tabletop scanning micro X-ray fluorescence (μ-XRF) analyzer in the Geosciences Department at the UA was also used to determine the distribution of major and trace elements in rock and sediment samples. Measurements of elemental count rates were made over a 15 s integration time at 100 μm spacing along two line scans spanning pellets of compressed sample material (keV = 40, μA = 400). The crystallography of carbonate material within the sediment traps was also assessed through both microprobe and X-ray diffraction analysis (the latter on a Bruker X8 Apex diffractometer in the Mineralogy and Crystallography Laboratory at University of Arizona). Finally, the percentage of biogenic silica in the sediment trap samples was measured by spectrophotometry at Northern Arizona University following wet alkaline extraction (10% Na_2CO_3) and molybdate-blue reduction [*McKay et al*., 2008 after *Mortlock and Froelich*, 1989].

3.1.4. Sediment Record

We collected short and long cores from the lake to extend the sediment record from cores collected in December 1991 [*Riedinger et al*., 2002]. Three cores were collected in 2007 using a Colinvaux-Vohnout

piston corer, and four additional short (~77 cm to ~99 cm long, ~4 cm diameter) sediment cores were taken in December 2009 using an Aquatic Research Instruments Universal Percussion Corer with a 1 m long sampling tube (~7 cm diameter). The sediment cores were collected from the deepest section of the lake in approximately 3–3.2 m water depth. The sediment-water interface was preserved in each core, and we extruded the uppermost portion in the field due to their high water content. All cores and sediment trap samples were stored in a cold room at 2 ± 1°C (36 ± 2°F) prior to analysis.

Samples from the 2009 sediment core were embedded in epoxy resin, and measurements of elemental count rates were made down seven parallel scans of the sediment core at 100 μm increments with the μ-XRF over a 15 s integration time (KeV = 40, μA = 400). Elemental count rates were normalized to potassium (i.e., Si/K, S/K, Cl/K, Ca/K, Ti/K, Fe/K, and Sr/K) to remove variability associated with the thickness of the embedded sediments. Empirical orthogonal function analysis was performed in MATLAB on the correlation matrix of μ-XRF K-normalized count rates [*Weare et al*., 1976; *Peixoto and Oort*, 1992, Appendix B] to find the dominant mode of elemental variability within the Bainbridge sediment record. Two gaps in the XRF record occur where unconsolidated gypsum gravel could not be embedded in epoxy resin.

A GEOTEK core logger at the University of Florida Land Use and Environmental Change Institute generated high-resolution photographs of the 2007 cores for gray scale analysis. A composite was created from the images of the two longest cores to obtain a record free of slumping. A record of sediment color changes was produced from the composite images using Image J v. 1.0 gray scale analysis software [*Rasband*, 2004]. Samples for pollen analysis were also taken from the longest (~3.6 m) 2007 core during periods of color and sediment composition transitions (n = 30, 0–170 cm). Samples were treated using standard pollen preparation protocols [*Faegri and Iversen*, 1989], and each sample was spiked with polysterene microspheres (5000 for 0.5 cm^3 and 10,000 for 1 cm^3samples) to calculate pollen concentration [*Battarbee and Kneen*, 1982]. Due to the restricted flora and very low productivity (average 121 grains/cm^3) at Bainbridge, pollen counts were conducted until 100 pollen grains or 2000 microspheres were counted and converted to pollen concentration to account for differences in sample volume. Pollen concentrations were grouped into local (*Sesuvium* sp. and *Croton* sp.) and regional (other) sources to separate the local rainfall-driven vegetation response and the regional wind-driven pollen signal.

All analyses presented were performed on the 360 cm 2007 core and the 92 cm 2009 core, as these cores were the longest and displayed the most distinct laminations. Results from these new cores were also compared to the 415.8 cm core collected in 1991 [*Riedinger et al*., 2002]. For clarity, cores will be referred to by their year of collection throughout the remainder of the paper (i.e., the "1991," "2007," and "2009" cores).

3.2. Age Modeling

Dating constraints from ^{210}Pb and ^{137}Cs proved impossible, as their activities were too low to be detected in these sediments. This same limitation has been reported in dating other lowland Galápagos lakes and likely stems from the fact that the lowland lakes receive very little rainfall and therefore very little input of atmospheric ^{210}Pb (*M. Brenner*, personal communication, 2013). In contrast, higher atmospheric deposition via rainfall and garúa (light rain at 500–1000 m elevation from the formation stratocumulus clouds during the dry season) permits ^{210}Pb and ^{137}Cs dating of highland lakes (e.g., El Junco) [*Conroy et al*., 2008].

We established an age model for the sediment record through radiocarbon dating of bulk sediment samples using accelerator mass spectrometry (AMS) at UA. We obtained 10 bulk sediment radiocarbon dates from the 2009 core and 4 bulk sediment radiocarbon dates from the 2007 core. Dissolved inorganic carbon (DIC) in a water sample collected in October 2012 from 3 m depth was used to determine the reservoir age of the lake. An acid-only pretreatment was used for the bulk sediment samples, which were combusted and measured for radiocarbon content at the National Ocean Sciences AMS Facility (2007 core) and the UA AMS Laboratory (2009 core).

The *Bacon* package v2.2 in R [*Blaauw and Christen*, 2011] was used to calibrate the radiocarbon dates and produce age-depth models for each core. By incorporating prior knowledge of sedimentation rate and reconstructing the sedimentation rate itself, this method produces improved age-depth models over other conventional age modeling techniques. We assumed a mean accumulation rate of 20 yr/cm and used the Marine13 calibration curve [*Reimer et al*., 2013], the Southern Hemisphere Zone 1–2 postbomb calibration

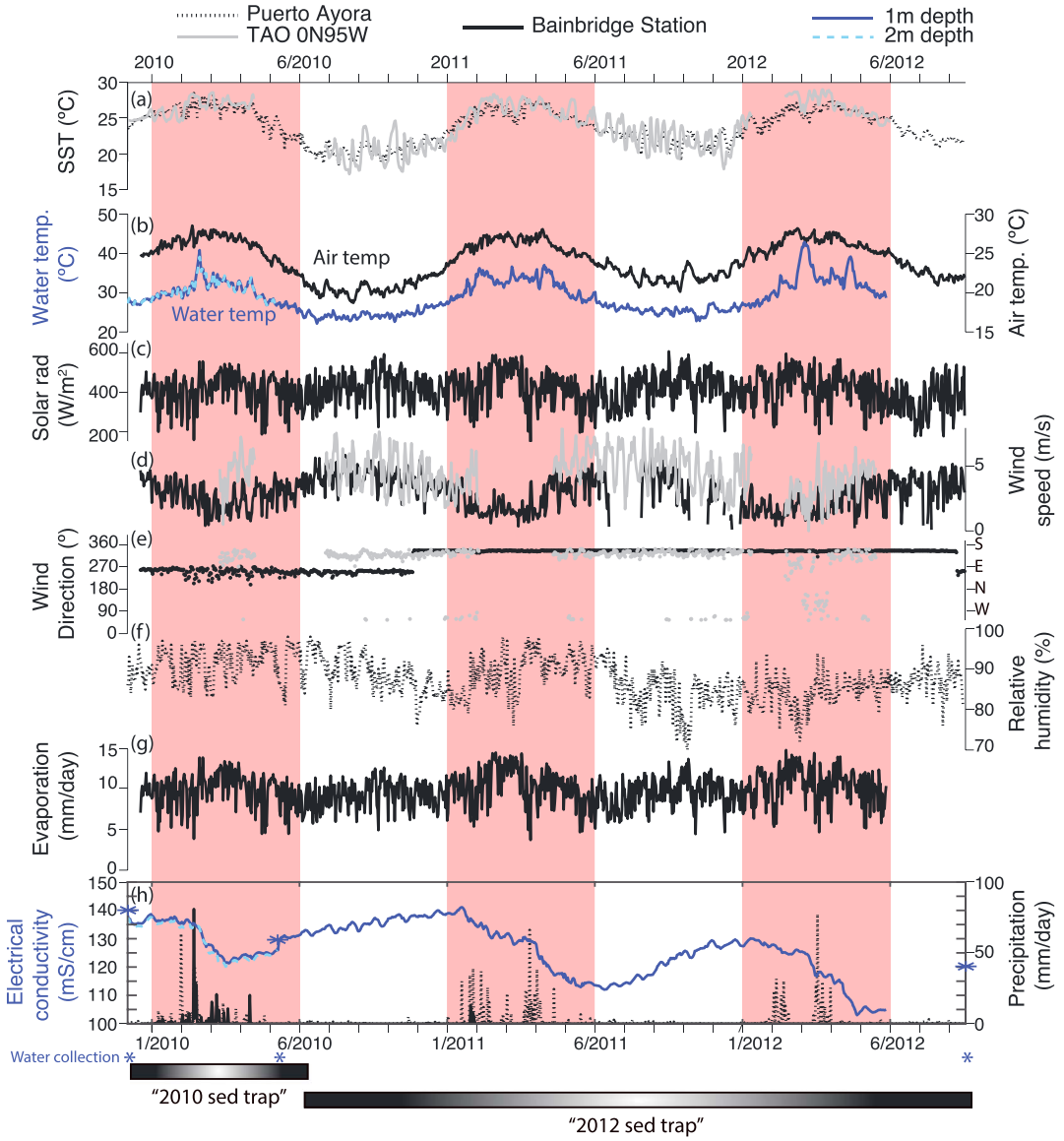

Figure 2. Local climate and limnology over entire study period. Time series of daily average (0:00–23:45 h) local climate and limnology for the study period: 2 December 2009 to 3 October 2012. (a) Sea surface temperatures (SST, °C) from Puerto Ayora (black dashed) [*Charles Darwin Foundation*, 2012] and a Tropical Atmosphere Ocean (TAO) array station at 0°N, 95°W F; gray). (b) Air temperature recorded by the Bainbridge weather station (black) and water temperature at 1 m (blue solid) and 2 m (blue dashed) depth recorded by AquaTroll 100 sondes. (c) Average daytime solar radiation measured from the weather station (W/m^2). (d) Wind speed recorded by the weather station (black) and by the TAO array at 0°N, 95°W (gray). (e) Wind direction (ϕ_{vect}, degrees) recorded by the weather station (black) and by the TAO array at 0°N, 95°W (gray), where ϕ_{vect} = 0/360 = toward the north or southerly wind (ϕ_{met}, as indicated on the second *y* axis: southerly, easterly, westerly, and northerly). (f) Percent humidity recorded at Puerto Ayora. (g) Evaporation at the lake surface in mm/d calculated from local air temperature, lake temperature, solar radiation, and wind speed along with relative humidity from Puerto Ayora using the energy budget equation [*Shuttleworth*, 1993]. (h) Precipitation (mm/d) at Bainbridge (black) and Puerto Ayora (black dashed) along with (specific) electrical conductivity (mS/cm) of the lake measured at 1 m (blue solid) and 2 m (blue dashed) depth and in surface water samples (blue stars) collected on 1 December 2009, 6 June 2010, and 3 October 2012. The two sediment trap periods (2 December 2009 to 6 June 2010 and 6 June 2010 to 2 October 2012) and water collection dates (1 December 2009, 6 June 2010, and 3 October 2012) are indicated at the bottom of the figure, and the warm seasons (1 January to 31 May) are highlighted in red.

curve [*Hua et al*., 2013], and an offset based on the reservoir age of the lake calculated from the DIC of the 2012 3 m water sample. Calibrated ^{14}C ages and 2σ weighted average standard deviations were reported in calendar years B.P. (with respect to A.D. 1950) and reported along with corresponding calendar years since the start of the Common Era (CE). The "best" age models, based on the weighted mean age of the Markov chain Monte Carlo (MCMC) iterations for each depth, were used to develop the core chronologies.

3.3. Updated Bainbridge Laminae Record

New sediment core records from Bainbridge were compared with the record of laminae counts from the 1991 core [*Riedinger et al*., 2002]. For this comparison, we compiled laminae in the 1991 core into 250 and 500 year bins to assess millennial-scale ENSO variability over the past 6000 years. Following the age-modeling approach described above, we modified the chronology for the 1991 core using the updated ^{14}C correction for the reservoir age of the lake.

4. Results

4.1. Physical Monitoring Data

Daily average air temperature reached 26–28°C in the warm/wet season and fell as low as 19°C in the cool/dry season during our monitoring period (Figures 2, S2, and Table S1). Solar radiation and evaporation were greater during the warm/wet season, with a daily average of ~450 W/m^2 and ~11 mm/d, respectively, compared with ~420 W/m^2 and 9.5 mm/d during the cool/dry season. Stronger winds were observed in the cool/dry season, with a daily average of ~4 m/s and gusts of up to 10 m/s. Precipitation at the lake fell almost exclusively in the warm/wet season when daily air temperatures rose above 24°C, with an average of ~1 mm/d and a maximum of 80 mm/d during the 2009–2010 El Niño event. Although no precipitation was recorded at Bainbridge during the 2012 El Niño warm season, an average of ~2.9 mm/d (435 mm total) was recorded at Puerto Ayora station (Figure 1). As the precipitation data at Bainbridge and Puerto Ayora were correlated during the initial logging period (18 December 2009 to 5 June 2010; Spearman's rank correlation: $r_s = 0.49$, $N = 170$, $P < 0.001$), the absence of precipitation during the moderate 2012 El Niño may be an artifact or a malfunction of the Bainbridge rain gauge. Nonetheless, as Bainbridge lies on the leeward side of Santa Cruz, where much of the moisture associated with the SE trade winds is deposited in the highlands (Figure 1a) [*Hamann*, 1979; *Pryet et al*., 2012], it is conceivable that Bainbridge received little if any rainfall during this period. We include Puerto Ayora station data in all precipitation analyses as a conservative estimate of precipitation during this period.

Bainbridge Crater Lake was well mixed by strong southeasterly trade winds blowing throughout the monitoring period (Figure 1b). Stratification was not observed in either the YSI profiles collected from the deepest portion of the lake on the afternoon of 6 June 2010 (Table S2) or between the temperature and conductivity at 1 and 2 m depth (Figure 2). The lake displayed strong seasonality in response to the local climatology, with strong differences (warm/wet-cool/dry) in temperature, salinity, and density between seasons (Figures 2, S3, and Table S1). Daily average water temperatures lagged behind air temperature due to the heat capacity of the lake, and the daily average electrical conductivity maximum lagged water temperature minimum of the cold/dry season by 1 to 2 months in response to changes in the local precipitation minus evaporation (P − E) balance. Conductivity of the lake was strongly negatively correlated with both air and water temperature and positively correlated with wind speed over the monitoring period (Table 1). In contrast, precipitation, evaporation, and the overall P − E budget were not associated with lake conductivity (Table 1).

Interannual variability associated with ENSO events was observed during the warm seasons (Figures S4, S5, and Table S3). The warm season of 2010, a weak El Niño year, was wetter than the other two warm seasons at Bainbridge. A total of 300 mm of rain fell at Bainbridge during the 2010 warm season, compared with 24 mm in the 2011 and 0 mm in the 2012 warm season. Daily average evaporation at the lake was lower, and the overall P − E budget was more positive during the weak 2010 El Niño than in the other warm seasons (Figure S4). Although daily average salinity and water density were lower in the 2010 warm season than in the 2011 warm season, the lowest values were observed over the 2012 warm season (Figure S5 and Table S3).

Table 1. Correlations Between Climate and Limnological Data[a]

	Precip Bain	Precip PA	Air Temp	Wind Speed	Tot. Rad.	Evap	P − E Bain	P − E PA	Water Temp	Spec. Cond	Salinity	Density
Precip Bain	1	0.20***	0.19***	−.08*	0.17***	−0.09***	0.28***	0.18***	0.16***	0.12***	0.13***	0.08***
Precip PA		1	0.10***	−0.03	−0.16***	−0.20***	0.23***	0.56***	0.11***	0.04	0.06*	0.01
Air temp			1	−0.42***	0.38***	0.34***	−0.29***	−0.14***	0.93***	−0.24***	−0.20***	−0.39***
Wind speed				1	−0.05	−0.06*	0.04	−0.02	−0.37***	0.23***	0.22***	0.27***
Tot. rad					1	0.70***	−0.63***	−0.59***	0.29***	0.10***	0.12***	0.05
Evap						1	−0.97***	−0.84***	0.32***	−0.05	−0.04	−0.10***
P − E Bain							1	0.84***	−0.27***	0.06*	0.05	0.1***
P − E PA								1	−0.13***	0.06*	0.06*	0.07**
Water temp									1	−0.28***	−0.23***	−0.44***
Spec. cond										1	1.0***	0.98***
Salinity											1	0.97***
Density												1

[a]Spearman's ρ correlation coefficients between climatic and limnological conditions at Bainbridge Crater Lake.
*Significant at 90% confidence level.
**Significant at 95% confidence level.
***Significant at 99% confidence level.

The two sediment trap sample periods (Figure 2) were characterized by distinctly different climates and lake conditions (Table S4), as they were composed of different portions of the local wet and dry seasons as well as different phases of ENSO. The local climate and limnology were more variable during the 2010–2012 ("2012") sediment trap period than in the December 2009 to June 2010 ("2010") sediment trap period (Figure 3). Nonetheless, the 2010 sediment trap period was warmer and wetter, with higher humidity, weaker winds, and a more positively skewed P − E budget than the 2012 sediment trap period (Figure 3c and Table S4). The lake was warmer and less dense during the 2010 sediment trap period than during the 2012 period (Figure 3 and Table S4). Linear mixed modeling suggests that there was a significant impact of sampling period on local climate and limnology, with the 2012 sampling period being significantly cooler and drier and with higher water density and salinity in the lake (Table 2). There was also a significant impact of season on local climate and limnology and a significant interaction between sampling period and season for Bainbridge precipitation, solar radiation, evaporation, precipitation-evaporation, EC, density, and salinity (Table 2).

4.2. Water Chemistry

The oxygen isotopic composition of the lake reflects evaporation at the lake, enriching the lake water ($\delta^{18}O_{mean}$ = 3.37‰) relative to seawater ($\delta^{18}O_{mean}$ = 0.059‰) and local precipitation (long-term $\delta^{18}O_{mean}$ = −1.91‰). Chemical analysis of the lake water samples collected on 1 December 2009, 6 June 2010 (bracketing the warm/wet season and a weak El Niño; Figure 2), and 3 October 2012 (cool/dry season following a prolonged La Niña and moderate El Niño; Figure 2) provided the following evidence of wetter conditions during the 2010 sediment trap collection period and drier conditions during the 2012 collection period (Table S5). The 2010 water samples were characterized by lower concentrations of cations and anions (e.g., Na, Si, Cl, and SO_4) at the surface than at depth. Bicarbonate concentration also decreased throughout the water column in 2010 compared to 2009 and 2012. In contrast, the 2012 water samples were characterized by high bicarbonate concentrations, a lack of chemical stratification with depth, and high DIC.

4.3. Composition of Sediments From Sediment Traps

Sediments that accumulated within the sediment traps consisted of both autochthonous (e.g., carbonate and organic matter) and allochthonous (e.g., terrigenous sediment and pollen) components. The composition and abundance of trace elements in the sediment trap sediments (Figure S1) differed between sampling periods and from that of the parent rock.

Microprobe mapping of a rock sample collected from the crater rim (Figure S6a) and μ-XRF intensities of major and minor trace elements in five rock samples and one soil sample support the identification of the

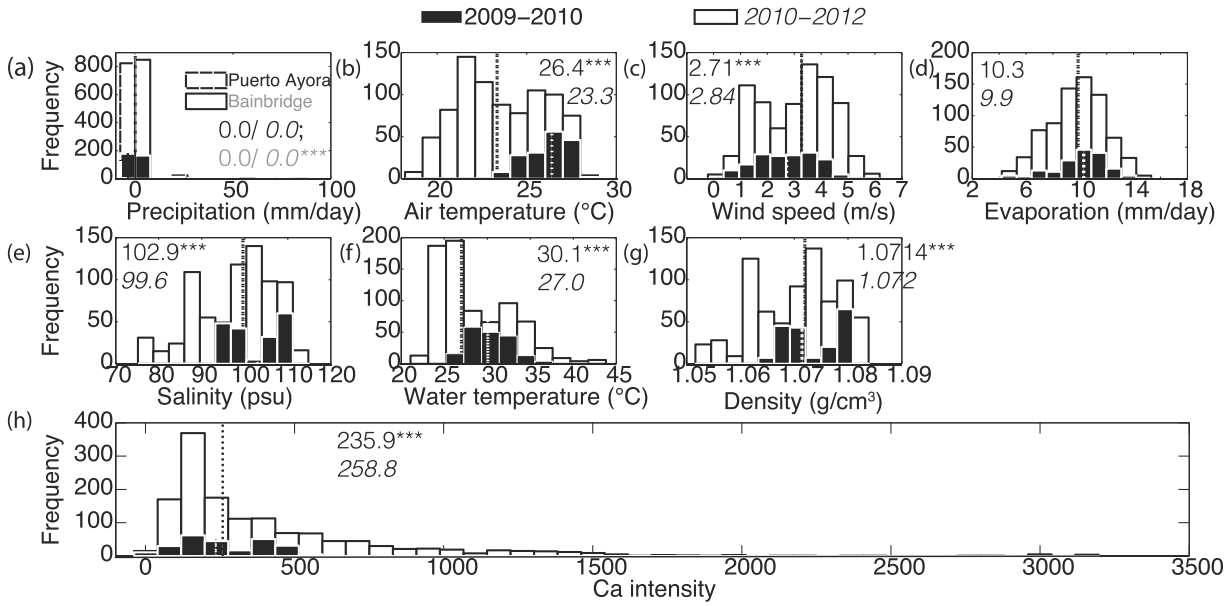

Figure 3. Comparison of Bainbridge climate and limnology between 2010 and 2012 sediment trap periods. Histogram of daily average (a) rain, (b) air temperature, (c) wind speed, (d) evaporation, (e) salinity, (f) water temperature, and (g) density at 1 m depth, along with (h) the distribution of sediment micro X-ray fluorescence (μ-XRF) calcium intensities (see methods for "Sediment sampling and analyses") of the 2010 sediment trap sample (2 December 2009 to 5 June 2010, black with normal font) and the 2012 sediment trap sample (6 June 2010 to 2 October 2012, white with italic font). The median value (Table S4) is listed and denoted by a dotted line on each histogram (of contrasting color: white dotted for 2009–2010 and black dotted for 2010–2012). Asterisks denote that the linear mixed effect model indicated that the two sampling periods were different at the 90% (single asterisk), 95% (double asterisks) and 99% (triple asterisks) confidence level, respectively.

Table 2. Linear Mixed Effects Model Results[a]

		Season (Warm/Wet-Cold/Dry)		Sample (2012–2010)		Interaction (Season × Sample)	
		χ^2	Δ Rank	χ^2	Δ Rank	χ^2	Δ Rank
Air temperature (°C)		818.0***	403.4	151.9***	−238.3	3.7	106.2
Precipitation (mm/d)	Bainbridge	3.3	13.4	68.6***	−95.3	25.4***	118.3
	Puerto Ayora	15.5***	73.1	0.112	−8.2	0.78	59.8
Puerto Ayora humidity (%)		0.19	9.0	20.1***	−154.4	0.01	10.2
Wind speed (m/s)		65.0***	−166.2	12.2***	119.8	2.9	176.5
Total solar radiation (W/m^2)		49.1***	119.3	158.9***	−404.3	7.9**	173.0
Evaporation (mm/d)		56.8***	172.0	2.2	41.9	5.5*	147.9
Precipitation-evaporation (mm/d)	Bainbridge	180.9***	−291.1	36.1***	−210.4	19.4***	400.2
	Puerto Ayora	57.7***	−170.6	11.3***	−125.3	12.8***	325.2
Water temperature (°C)		506.1***	5.63	6.1***	−0.77	3.2	1.5
Electrical conductivity (mS/cm)		305.8***	10.4	309.4***	15.7	9.7**	7.8
Density (g/cm^3)		164.8***	0.0059	282.6***	0.012	6.6*	0.0052
Salinity (psu)		338.1***	10.5	309.5***	14.9	9.9**	7.51

[a]A linear mixed effects model was used to assess the relationship between rank-transformed meteorological and limnological conditions and both sampling period and season using the lme4 package [*Bates et al.*, 2015] in *R* (R Core Team 2016), with sampling year as a random effect to account for repeated measurements. A likelihood ratio test (χ^2, d.f. = 1, N = 1020 for meteorological data and N = 939 for limnological data) was used to assess the impact of season and sample period and the interaction between the two, on each variable. The change in rank between seasons (warm/wet to cool/dry), sampling period (2012 to 2010), and their interaction is denoted by Δ Rank.

*Significant at 90% confidence level.
**Significant at 95% confidence level.
***Significant at 99% confidence level.

parent material as Fe, Mg (mafic) scoria basalt [*Swanson et al*., 1974]. The Bainbridge soil sample was identified as a torrand, an andisol common to arid climates [*Soil Survey Staff*, 2010] and observed in other parts of the Galápagos archipelago [*Franz*, 1980]. The soil sample and rock samples with visible evidence of weathering displayed significantly higher Al/Si ratios than in the parent rock (Figure S7; Kruskal Wallis: $H = 216.3$, $N = 495$, $P < 0.001$; Mann-Whitney U: $U_{soil\text{-}rock} = 9.98$, $N = 168$; $P < 0.001$), consistent with enriched Si in the lake relative to sea water and confirming greater leaching of Si than Al during chemical weathering.

The sediment trap samples from 2010 and 2012 were both rich in organic matter, including high abundances of biogenic silica from diatom frustules. However, Si was more concentrated in 2012 (7.8–9.9%) than in 2010 (4.9%). Counts of major constituents in 0.25 cm^3 aliquots of the sediment trap samples under 200–300X stereoscopic magnification further suggested a higher content of organic matter (algae, *Chironomidae sp*., arthropod remains, and fecal pellets) in 2012 than in 2010 (Table S6 and Figures S8d–S8f).

The 2010 sediment traps displayed high concentrations of Si, K, Na, and Mg (Figure S6b) and low concentrations of Ca. In contrast, Ca was abundant throughout the 2012 sediment trap samples (Figures S6c, S6d, and S9). The μ-XRF Ca intensities (paired, not normally distributed data) were significantly different between the two sediment trap periods (2010 and 2012), with a higher median and more positively skewed distribution in 2012 compared with 2010 (Mann-Whitney U: $Z = -3.64$, $N = 1630$, $P < 0.001$; Figure 3i). Examining the crystallography of this carbonate material using microprobe and through XRD analysis revealed that the carbonate precipitating in the lake during the 2012 sediment trap period was primarily composed of magnesium-rich calcite and aragonite (Figures S8g–S8i and S9). In 2012, a < 1 mm thick layer of plate-like carbonate (Mg-rich calcite and aragonite) also precipitated on the walls of the sediment traps (Figures S1, S7d, S8j–S8l, and S9c).

4.4. Age Model

The average sedimentation rate from the resulting radiocarbon age models was between 0.07 and 0.14 cm/yr, with variability through time (Figures 4 and S10). There was no evidence of a hiatus in the sediment record from these cores. Radiocarbon dating of the DIC in a water sample collected from 3 m depth in 2012 suggests a reservoir age of 87 ± 35 ^{14}C years (Table S7), indicating that both atmospheric and seawater sources contribute to the lake carbon reservoir.

4.5. Lithology

All cores displayed two ~12 cm thick sections of coarse gypsum gravel (grain size of 1–8 mm) starting at ~4–6 cm and ~20–22 cm depths, deposited on top of alternating light (carbonate, Ca/Sr rich) and dark brown (siliciclastic, Si/Fe rich) laminations (Figures 4a and S11). Sediments between these gypsum layers were composed of a light brown to olive-green organic-rich matrix. Gypsum gravel was rare or absent from the remainder of the sediment record. The dominant mode of variability observed in the μ-XRF elemental intensity correlation matrix (principal component 1, PC1, explaining 32% of the variance) displayed strong positive loadings for S, Ca, and Sr (eigenvectors: 0.52, 0.61, and 0.41, respectively) and negative loadings for Si and Fe (eigenvectors: −0.32 and −0.25, respectively). High variability in gray scale values and pollen abundance and origin co-occurred with these changes in sediment composition (Figure 5), with moderate to high gray scale values and regional/mainland pollen in the carbonate and gypsum sediments and low gray scale values and local pollen in the brown-green organic-rich and siliciclastic sediments. We observed no effect of either sedimentation rate or sample resolution on pollen concentration.

Below the level corresponding to ~1500 calendar years B.P., there were generally few carbonate and siliciclastic laminations, with the exception of two carbonate deposits around 6000–5500 (the base of the sediment record collected) and 3500–3000 years B.P. (Table S8 and Figure 6). Moderate gray scale values and roughly equal numbers of carbonate and siliciclastic laminae were observed between ~3000 and ~1500 calendar years B.P. (550 before the Common Era to 450 Common Era (C.E.)). Around ~1500 calendar years B.P. (450 C.E.), the Bainbridge sediment record displayed an increase in the mean and variability of gray scale values, an increase in the number of carbonate laminations, and a decrease in the number of siliciclastic laminations [*Riedinger et al*., 2002]. This sediment regime, with lighter-colored, more variable sediments and pollen concentrations and a peak in the number of carbonate laminations, persisted until ~700 calendar years B.P. (1250 C.E.) [Figure 5] when siliciclastic laminations began to increase, pollen concentration

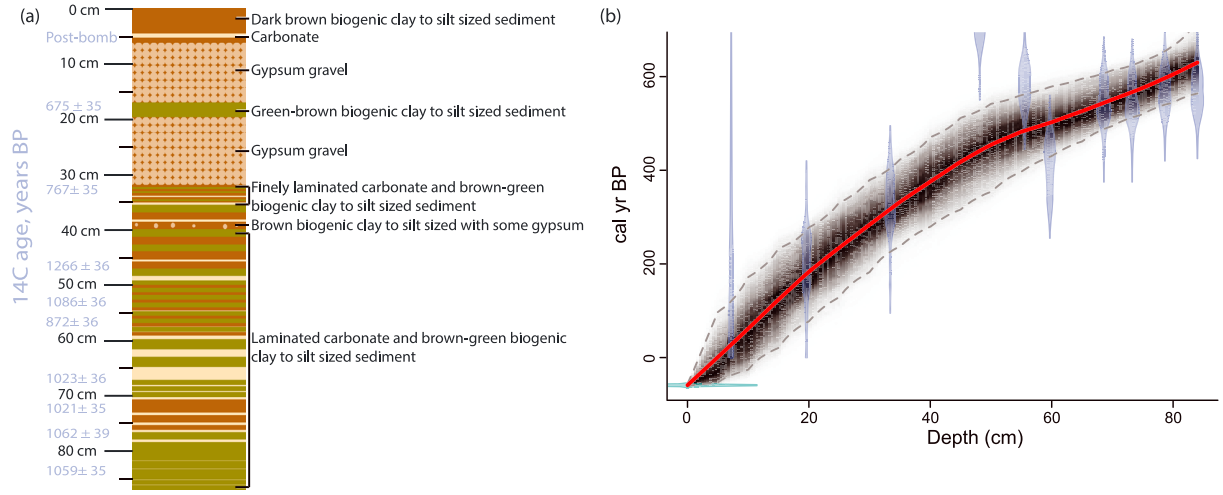

Figure 4. Lithology and age model for 2009 Bainbridge Crater Lake core. (a) Schematic of the lithology and radiocarbon age (^{14}C age, years B.P., where the "postbomb" sample had a fraction modern carbon of 1.1645 ± 0.0049, see Table S7) of the top ~87 cm of the 2009 Bainbridge Lake sediment core from which the micro X-ray fluorescence (μ-XRF) record was developed (see Figure S11 for photographs of the full sediment record of each core). (b) Bainbridge *Bacon* [*Blaauw and Christen*, 2011] age-depth model for the 2009 core (see Figure S10 for other age models), where blue markers indicate the calibrated ^{14}C dates, gray shading depicts the Markov chain Monte Carlo (MCMC) iterations, darker grays indicate more likely calendar ages, gray stippled lines depict the 95% confidence intervals, and the red line depicts the best age model based on the weighted mean at each depth.

decreased, and sediments became darker overall. This interval was punctuated by high PC1 values (associated with gypsum and carbonate minerals) between ~300 and 50 calendar years B.P. (1650–1900 C.E.). In contrast, low PC1 values were observed in the Bainbridge sediment record since 50 calendar years B.P. (1900 C.E.; Figure 5).

5. Discussion

Sediment trap samples from 2010 spanned a weak El Niño event and warm, wet conditions. The 2010 samples consisted primarily of brown-green, organic-rich sediments, with very little carbonate. The sediments were therefore dominated by the major elements of local rocks and soils (Fe, Si, K, Na, and Mg). In contrast, organic matter and carbonate were both abundant in sediment trap samples from 2012, collected during a period that was significantly cooler and drier and had stronger winds. Higher abundances of organic matter in the 2012 samples are consistent with stronger upwelling and higher nutrient availability in the eastern Pacific and the Galápagos during the cool, dry season and La Niña events [*Wyrtki*, 1981; *Kessler*, 2006]. This elevated regional nutrient variability may increase productivity in the lake as a result of the influx of seawater into the lake, which may be higher during cool, dry periods when high regional sea level pressure (SLP) increases the pressure gradient and thus seawater influx into the lake.

Although a number of mechanisms may drive carbonate formation in Bainbridge over the 2012 sediment trap period, high bicarbonate concentrations and a lack of chemical stratification with depth are consistent with dry conditions and strong trade wind-driven vertical mixing of the lake. In contrast, the lower concentrations of bicarbonate, cations, and anions (e.g., Na, Si, Cl, and SO_4) at the surface than at depth are consistent with high precipitation and diatom productivity (depleted Si) in 2010. Nonetheless, the longer sampling period likely contributed to the higher abundance of carbonate and organic matter in the 2012 sediment traps, as this sampling period consisted of two full seasonal cycles, an 18 monthlong La Niña event, and a moderate El Niño event. We found a significant influence of both season and sampling period on both the climate and limnology, as well as a significant interaction between the two for some key variables (Table 2). Therefore, the differences in sedimentation in the lake between these two sediment trap sampling periods may be attributed to both seasonal and interannual variability.

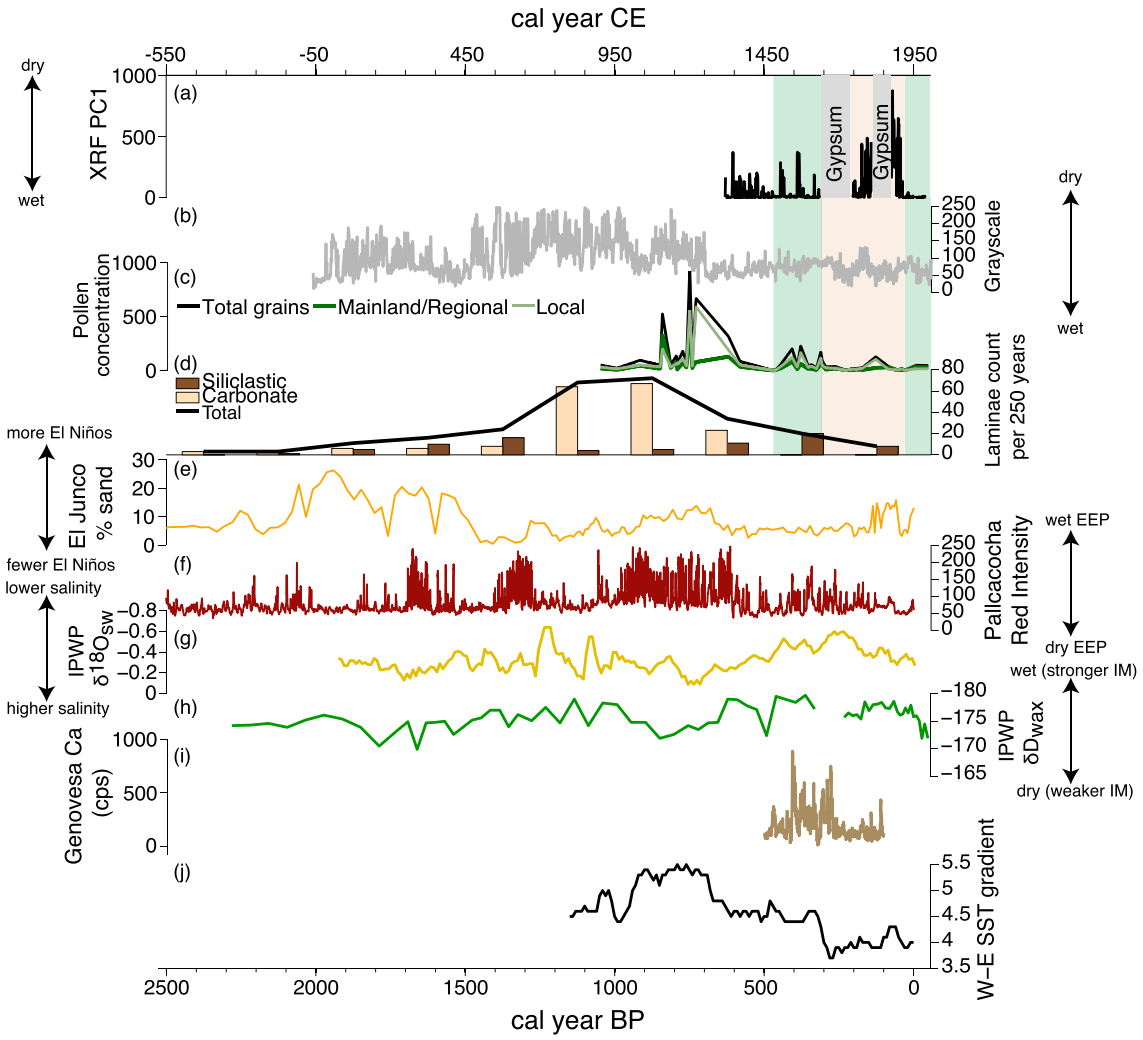

Figure 5. Comparison of tropical Pacific climate reconstructions over the past 2500 ka. Bainbridge sediment record: (a) The first principal component (PC1) of micro X-ray fluorescence (μ-XRF) intensity ratios. (b) Gray scale record (where high gray scale values indicate lighter colors). (c) Total, local (*Sesuvium* sp. and *Croton scouleri*) and regional (other) pollen concentration. (d) Carbonate and siliciclastic laminae (as in *Riedinger et al.* [2002]) counted in 250 year bins (and centered on the bin midpoint). Carbonate laminations (with high gray scale values) reflect precipitation of autochthonous calcite and/or aragonite due to evaporative forced oversaturation of the lake water during cool/dry periods, while siliciclastic laminae (with low gray scale values) reflect brown-green organic-rich sediments characteristic of warm/wet periods in the lake. High abundances of local pollen reflect warm/wet periods, while regional and mainland pollen indicate strong winds (associated with cool/dry periods). See text for further discussion. Other regional records are as follows: (e) El Junco percent sand [*Conroy et al.*, 2008], (f) Laguna Pallcacocha red color intensity (terrestrial runoff) [*Moy et al.*, 2002], (g) Indo-Pacific warm pool (IPWP) $\delta^{18}O_{sw}$ reconstruction [*Oppo et al.*, 2009], (h) IPWP δD leaf wax reconstruction of Indonesian Monsoon (IM) variability [*Tierney et al.*, 2010], (i) μ-XRF calcium counts per second in the Genovesa sediment record [*Conroy et al.*, 2014], and (j) zonal SST gradient reconstruction [*Conroy et al.*, 2010] between the IPWP [*Oppo et al.*, 2009] and eastern equatorial Pacific [*Conroy et al.*, 2009]. Shading denotes wet (green) and dry (tan) intervals at Bainbridge discussed in the text.

Carbonate precipitation in the hypersaline Galápagos crater lakes is controlled by a number of different factors. First, authigenic carbonate may precipitate as temperatures increase, as CO_2 is less soluble at higher temperatures. The greater abundance of carbonate during the 2012 sediment trap period, when temperatures were significantly cooler overall, suggests that temperature is not the primary driver of carbonate precipitation in this lake.

Authigenic carbonate precipitation may also occur during dry periods, when strong evaporation relative to precipitation concentrates ions, including calcium and carbonate, within the lake. In the same way, a reduction in seawater influx may also contribute to the concentration of ions in the lake. The influx of seawater into the lake through fissures in the basalt may be regulated by the pressure gradient between the lake and

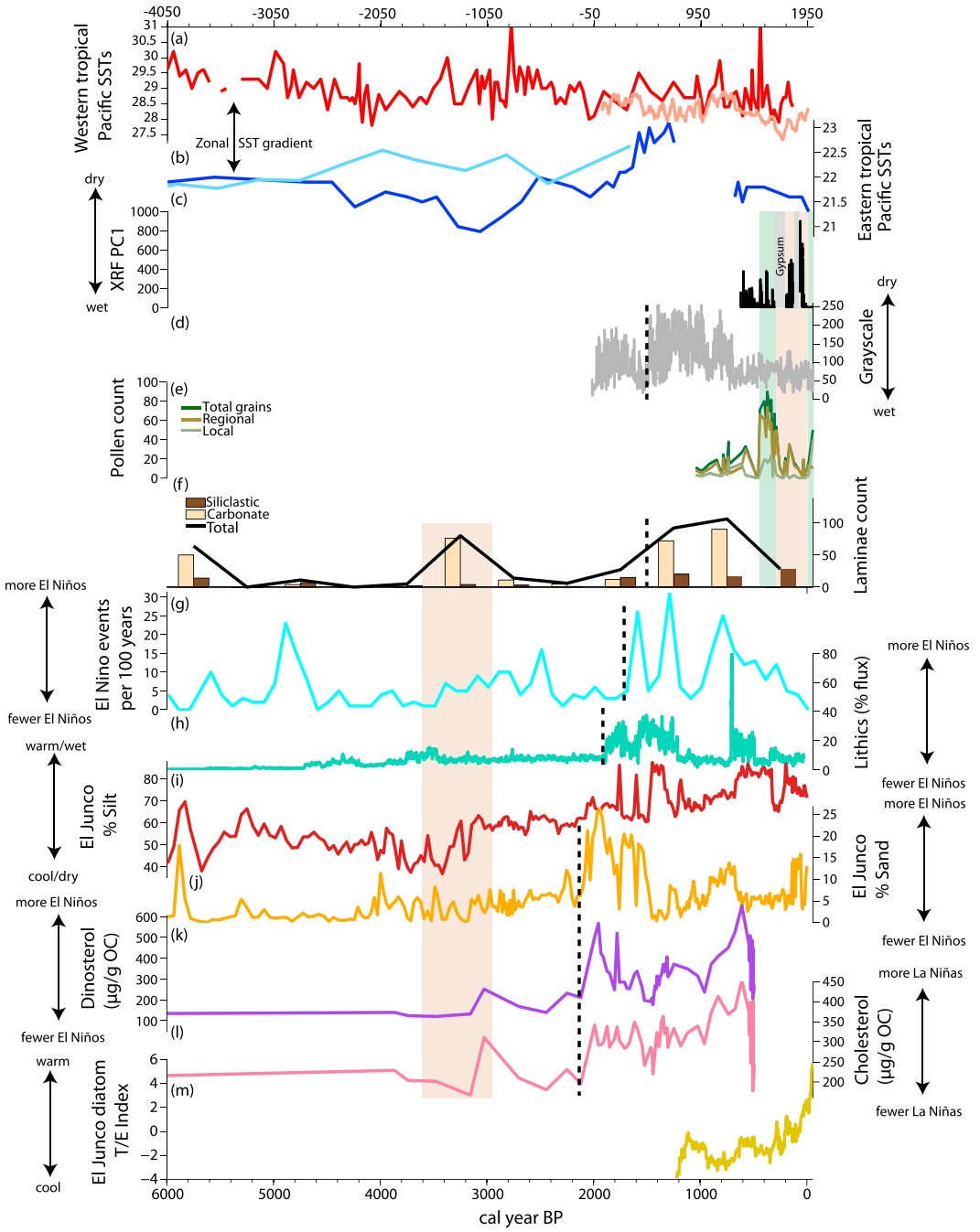

Figure 6. Comparison of tropical Pacific climate reconstructions over the past 6000 ka. (a) Western tropical Pacific sea surface temperature (SST) derived from foraminiferal Mg/Ca (red [*Stott et al.*, 2004]; light red [*Oppo et al.*, 2009]). (b) Eastern tropical Pacific SST derived from alkenones (blue [*Rein et al.*, 2005]) and from foraminiferal Mg/Ca (light blue [*Koutavas et al.*, 2002]). (c) Carbonate and siliciclastic laminae in the Bainbridge sediment record [*Riedinger et al.*, 2002] counted in 500 year bins. (d) Number of El Niño events in100 yr overlapping windows, Laguna Pallcacocha [*Moy et al.*, 2002]. (e) Lithic flux (% of max), Peru margin, with higher lithic flux suggesting more frequent El Niños [*Rein et al.*, 2005]; (f and g) Grain-sized records from lake El Junco (on nearby island of San Cristobal), where increased silt fraction occurs during warm/wet periods and higher sand fraction documents more frequent El Niños [*Conroy et al.*, 2008]. (h) Abundance of dinosterol (a dinoflagellate sterol that is sensitive to El Niño events [*Makou et al.*, 2010]). (i) As in Figure 6h for the abundance of cholesterol (eukaryotic sterol that is sensitive to La Niña events [*Makou et al.*, 2010]). (j) El Junco tychoplanktonic to epiphytic (T:E) diatom index, a proxy for regional sea surface temperature [*Conroy et al.*, 2009]. Dotted lines indicate the approximate timing of the dramatic increase in ENSO variability around 2 ka inferred from each record.

surrounding seawater as a result of regional SLP variability (e.g., associated with ENSO). Such pressure-related variations in lake level have been recorded at Genovesa Crater Lake, which is similarly weakly connected to the sea through fissures in the crater walls [*Conroy et al*., 2014]. This mechanism—authigenic carbonate precipitation as a result of the concentration of ions in solution—is consistent with significantly cooler, drier, and windier conditions resulting in cooler, more dense lake water and greater carbonate precipitation during the 2012 sampling period at Bainbridge Crater Lake (Table 2). Cool, dry La Niña conditions during this period were also associated with carbonate precipitation in Genovesa Crater Lake, another lowland Galápagos crater lake [*Conroy et al*., 2014].

However, cooler temperatures contributed significantly to the increased density observed across the 2012 sediment trap period (Table S4). Further, despite only small changes between the sediment trap intervals, electrical conductivity, salinity, and density displayed high interannual variability, with 2012 being the "freshest" period over the record. This suggests that the carbonate likely precipitated in 2011, when the salinity and density in the lake peaked. This strong interannual variability in local climate, limnology, and sedimentation in Bainbridge emphasizes the importance of such long monitoring data sets in the interpretation of the lake sediment record.

Lake conductivity was only strongly associated with (air and water) temperature and wind speed at the lake and not the local P − E budget (Table 1). This suggests a complex interplay between local climate (e.g., rainfall and *p*CO2), limnology, alkalinity, and carbonate precipitation that may be modulated through variations in pH, the influx of seawater, and productivity in the lake. In the next stage of this work, we will use the programs PHREEQC [*Parkhurst and Appelo*, 2013] and SUPCRT92 [*Johnson et al*., 1992] to investigate the carbonate solubility and saturation in response to variations in local climate and limnology, conductivity, and pH. Our working hypothesis is that the pH varies strongly in response to the local P − E budget (as rainwater lowers lake pH). pH in turn modulates carbonate precipitation in the lake, as carbonate saturation increases under more basic pH conditions [e.g., *Morse and Mackenzie*, 1990]. However, our results suggest that although pH, *p*CO2, and productivity play a role in mediating carbonate precipitation in this lake, they are of secondary importance to that of climatic controls on carbonate precipitation.

Increased primary productivity of calcareous organisms in the lake likely contributes significantly to biologically mediated carbonate precipitation [e.g., *Stabel*, 1986] during cool, dry, high-nutrient periods. Organic matter and biogenic silica content within the sediment traps were also greater during the 2012 sampling period, suggesting that biogenic and biologically mediated carbonate precipitation might contribute to higher carbonate precipitation during cool, dry periods. During these periods, we hypothesize that nutrient availability in the lake may rise as a result of increased regional upwelling of nutrient-rich waters, increased input of this nutrient-rich seawater to the lake (due to the increased pressure gradient), and increased guano deposition to the lake in response to increased nutrients, productivity, and marine seabird abundance. However, Si count rates were not correlated with Ca count rates over the A.D. 1320–1991 period, suggesting that either organisms driving biologically-mediated carbonate precipitation in the lake are out of phase with diatom abundance or that other processes besides productivity control carbonate precipitation in Bainbridge Crater Lake on longer timescales.

Regardless of the exact mechanism-driving carbonate precipitation in the lake, long-term monitoring of the climate and limnology of the lake over the 2009–2012 period indicate a need for a revised climate interpretation of the sediment record from Bainbridge. The results suggest that brown-green, organic-rich, siliciclastic laminae (associated with low PC1 and gray scale values and high local pollen abundance) in the Bainbridge sediment record reflect warm, wet conditions during wet seasons and/or El Niño events, when terrigenous material is washed into the lake via surface runoff from the crater walls and salinity of the lake decreases. In contrast, carbonate laminae and gypsum (associated with high PC1 and gray scale values and high regional/mainland pollen abundance) form during cool, dry conditions (associated with extreme dry seasons or La Niñas) when the lake temperature decreases and salinity increases. Further, we propose that prolonged dry conditions result in SO_4-rich water (with low HCO_3^- and excess Ca^{2+}), which favors gypsum precipitation relative to autochthonous carbonate. This proposed solute evolution is expected based on the excess of calcium ions relative to bicarbonate ions in solution in Bainbridge Lake (Table S5); as a result, bicarbonate ions are depleted as autochthonous carbonate

precipitates in the lake, leaving excess calcium ions to react with SO_4 to form gypsum during prolonged dry periods [see *Jones and Deocampo*, 2003]. The absence of a hiatus or change in sedimentation rate in the Bainbridge sediment record suggests that the lake did not dry up entirely during prolonged dry periods and that seawater influx into the lake maintained dissolved sulfate concentrations. Although the length of the monitoring period to date is not sufficient to definitively test this hypothesis for gypsum formation, these preliminary findings are consistent with geochemical analysis of sediment records from other saline lakes [*Mackenzie et al*., 1995; *Jørgensen and Cohen*, 2003; *Martín-Puertas et al*., 2011]. Finally, we interpret high concentration of nonlocal pollen grains (i.e., pollen from species that do not exist on Bainbridge that must have been transported by regional winds) to reflect an influx of pollen from surrounding islands and mainland South America by strong SE trade winds across the Galápagos Archipelago during La Niña conditions, whereas we interpret a high concentration of locally derived pollen grains to reflect increased abundance of local vegetation (*Sesuvium* sp. and *Croton* sp.) during wet periods.

Based on these long-term monitoring results, we compare the Bainbridge sediment record with other reconstructions of eastern Pacific ENSO variability [*Moy et al*., 2002; *Rein et al*., 2005; *Conroy et al*., 2008; *Makou et al*., 2010] and tropical Pacific SSTs [*Koutavas et al*., 2002; *Stott et al*., 2004; *Rein et al*., 2005; *Oppo et al*., 2009] to assess variability in the eastern tropical Pacific Ocean over the past 6000 years (Figures 5 and 6). The sensitivity and response to regional precipitation changes are likely to differ between lowland (Bainbridge and Genovesa) and highland (El Junco, Paul's Bog) Galápagos lakes. Therefore, discrepancies between records (where they exist) may be attributed at least in part to differences in their sensitivity to changes in seasonal versus interannual variability [*Koutavas and Joanides*, 2012] or lowland (convective) versus highland (garúa) rainfall [*Trueman and d'Ozouville*, 2010; *Wolff*, 2010], with lakes heavily influenced by garúa rainfall displaying a lagged response to regional climate variability relative to the dry lowland lakes. Differences in the local SST response—a result of heterogeneous oceanographic circulation and upwelling among the islands—may also be an important factor [*Liu et al*., 2013].

The Bainbridge sediment record supports reduced ENSO variability during the mid-Holocene in the eastern equatorial Pacific (Figure 6f) [*Moy et al*., 2002; *Riedinger et al*., 2002; *Koutavas et al*., 2006; *Conroy et al*., 2008; *Donders et al*., 2008]. With the exception of two periods around 6000–5500 and 3500–3000 calendar years B.P. few siliciclastic and carbonate laminations are observed in the Bainbridge sediment record between 6000 and ~1500 calendar years B.P. The moderate peak in siliciclastic and carbonate laminations around 6000–5500 calendar years B.P. suggests that ENSO events of both phases characterized this generally warm/wet interval, as inferred from the high percentage of sand and silt at El Junco Crater Lake [*Conroy et al*., 2008] (Figure 6) and increased lake level and mesic plant taxa in Paul's Bog on Santa Cruz [*Collins et al*., 2013]—both highland Galápagos lakes. In contrast, low percentages of sand and silt in the El Junco sediments and reductions in mesic plant taxa in Paul's Bog suggest only a moderate number of El Niño events and generally cool/dry conditions between 3500 and 3000 calendar years B.P. Therefore, the peak in carbonate laminations in Bainbridge during this period likely resulted from more frequent La Niña-related dry conditions. Additionally, this dry interval may have been associated with a strengthened Pacific E-W SST dipole [*Stott et al*., 2004; *Rein et al*., 2005]; however, the two eastern Pacific SST reconstructions [*Koutavas et al*., 2002; *Rein et al*., 2005] disagree over this interval (Figures 6a and 6b). Disagreement among records in the magnitude of mid-Holocene ENSO variability among the eastern (Figure 6f) [*Moy et al*., 2002; *Riedinger et al*., 2002; *Koutavas et al*., 2006; *Conroy et al*., 2008; *Donders et al*., 2008], central [*Cobb et al*., 2013; *McGregor et al*., 2013], and western tropical Pacific [*Corrège et al*., 2000; *Tudhope*, 2001; *McGregor*, 2004] suggests that mid-Holocene ENSO may have remained active but with a different spatial fingerprint than today [*Karamperidou et al*., 2015]. However, the bulk of the evidence from climate reconstructions across a diverse set of proxies in the eastern equatorial Pacific favors reduced canonical (classic or eastern Pacific type) ENSO variability during the mid-Holocene, as observed at Bainbridge Crater Lake [*Moy et al*., 2002; *Riedinger et al*., 2002; *Koutavas et al*., 2006; *Conroy et al*., 2008; *Donders et al*., 2008; *Karamperidou et al*., 2015].

The Bainbridge sediment record suggests an intensification of ENSO variability starting around 2000–1750 calendar years B.P. (Figure 6). ENSO variability began to slowly increase as early as 5000–4000

calendar years B.P. in some paleo-ENSO reconstructions, but large, contemporaneous increases in the number of both El Niño [*Moy et al*., 2002; *Rein et al*., 2005; *Conroy et al*., 2008; *Makou et al*., 2010] and La Niña events [*Makou et al*., 2010] occurred around 2000 calendar years B.P. (although the inferred timing of this climatic shift varies among records). We estimate the timing of this transition based on the mean (and associated uncertainty) of the climate shift across reconstructions and find that the marked increase in ENSO-related variability occurred around 1780 (± 230) calendar years B.P. This timing coincides with a change in vegetation community stability at El Junco Crater Lake, with more rapid oscillations between wet and dry conditions and plant community composition after 1800 calendar years B.P. (150 C.E.) [*Restrepo et al*., 2012]. SST reconstructions from the eastern and western tropical Pacific suggest that these changes in ENSO variability were coeval with a reduction in the strength of the E-W SST dipole [*Stott et al*., 2004; *Rein et al*., 2005; *Conroy et al*., 2008].

A peak in the number of carbonate laminations and high variable gray scale values between ~1500 and 700 calendar years B.P. (450 C.E.–1250 C.E.) suggests that frequent El Niño and La Niña events occurred during this interval. A moderate percentage of sand in El Junco [*Conroy et al*., 2008] and highly variable red intensity at Laguna Pallcacocha [*Moy et al*., 2002] are consistent with strong ENSO-related variability in the eastern Pacific during this period (Figure 5).

The gray scale and laminae records indicate a shift toward generally darker, less variable sedimentation in the lake after ~700 calendar years B.P. (~1250 C.E.), suggesting a decrease in the number of La Niña events and a corresponding decrease in the overall amplitude of ENSO-related variability, which occurred along with a weakening of the Pacific E-W SST dipole (Figure 6) [*Conroy et al*., 2010]. The deposition of siliciclastic laminae and high local pollen concentration around 410–330 calendar years B.P. (~1540–1620 CE) and after 50 calendar years B.P. (1900 CE) suggests that two periods of frequent El Niño-related wet conditions interrupted this interval of otherwise low ENSO activity (Figure 5).

The deposition of gypsum (Figure 5) and an absence of diatoms (Figure S12) suggest extreme, persistent dry conditions in the eastern equatorial Pacific between 300 and 50 calendar years B.P. (1650–1900 C.E.), consistent with few El Niño events and generally dry conditions inferred from the El Junco (% sand), Laguna Pallcacocha, and Genovesa sediment records (Figure 5) [*Moy et al*., 2002; *Conroy et al*., 2008, 2014]. Along with records from the western tropical Pacific, which indicate a stronger Indian monsoon and lower salinity during this interval [*Oppo et al*., 2009; *Tierney et al*., 2010], these hydrologically sensitive proxies suggest that this period was anomalously dry in the eastern equatorial Pacific and wet in the western Pacific (i.e., strong Pacific E-W dipole) [*Oppo et al*., 2009; *Tierney et al*., 2010; *Yan et al*., 2011]. These records, however, are in contrast to reconstructions that suggest a reduced E-W SST dipole (Figure 6) [*Cobb et al*., 2003; *Newton et al*., 2006; *Conroy et al*., 2009; *Oppo et al*., 2009; *Conroy et al*., 2010] and a southward displacement of the intertropical convergence zone (ITCZ) [*Sachs et al*., 2009] between 300 and 50 calendar years B.P. (1650–1900 C.E.), which would produce wetter conditions in the Galápagos. Hydrogen isotopic records from El Junco (1°S), Palau (7°N), and Washington Lake (5°N) suggest that the ITCZ shifted back northward between ~1550–1600 and 1850 C.E. [*Sachs et al*., 2009]. El Junco was therefore transitioning toward drier conditions during this interval when Bainbridge and Genovesa [*Conroy et al*., 2014] were dry, suggesting that a lagged response of highland lakes (e.g., El Junco) relative to lowland lakes (e.g., Bainbridge and Genovesa) may reconcile differences in the timing of the response of Galápagos lakes to changes in the position of the ITCZ (within the uncertainty of the age models for these records). The contribution of garúa rainfall may dampen or delay the response of highland lakes to shifts in the ITCZ and associated changes in wet season rainfall, resulting in a lagged response relative to lowland lakes. Further, modulations in the magnitude of seawater input to lowland lakes may also contribute to the observed difference in the sensitivity and timing of these lakes to regional hydrological variability.

While uncertainty in the sensitivity and interpretation of proxy records may contribute to the discrepancy among records, the difference between SST [*Moy et al*., 2002; *Cobb et al*., 2003; *Newton et al*., 2006; *Conroy et al*., 2009, 2010] and hydrological [*Moy et al*., 2002; *Conroy et al*., 2008; *Oppo et al*., 2009; *Tierney et al*., 2010; *Conroy et al*., 2014] proxy records suggests that the atmospheric and oceanic response to forcing on centennial timescales may not be as tightly coupled as with ocean-atmosphere feedbacks on interannual timescales [*Tierney et al*., 2010; *Clement et al*., 2011; *Yan et al*., 2011]. Alternatively, this pattern within the tropical Pacific (reduced SST gradient with wet western-central Pacific and dry eastern Pacific) could have

resulted from a restriction of El Niño-related precipitation anomalies to the central Pacific as observed during modern day El Niño Modoki events [*Ashok et al*., 2007; *Weng et al*., 2007]. This potential for decoupling between temperature and hydrological [*Bony et al*., 1997] variability during the last millennium suggests that further work is needed to investigate the mechanisms behind centennial-scale climate variability in the equatorial Pacific.

6. Conclusions

Based on long-term monitoring and additional short cores from Bainbridge Crater Lake, we provide a new interpretation of the lake sediment record in which carbonate and gypsum laminae reflect cool/dry conditions and siliciclastic laminae reflect warm/wet conditions. Ongoing monitoring at this lake will investigate the relative contribution of seasonal and interannual climate variability to these sedimentation patterns and assess the interplay between local climate, seawater influx, lake conductivity, pH, and carbonate precipitation. Nonetheless, our long-term monitoring results suggest that the laminations within the Bainbridge sediment record provide a record of ENSO events of both phases over the past 6000 years. The record supports a broad-scale reduction in ENSO variability in the eastern equatorial Pacific during the mid-Holocene, which was punctuated by a brief period of relatively high ENSO variability around 6000–5500 calendar years B.P. and a period of frequent La Niña events between 3500 and 3000 calendar years B.P. The Bainbridge sediment record then suggests an increase in ENSO variability starting around 1750–2000 calendar years B.P., with strong interannual variability of both phases persisting until ~700 calendar years B.P., when overall ENSO-related variability at the lake decreased as the tropical Pacific E-W SST dipole strengthened. Finally, the Bainbridge sediment core record provides support for dry conditions in the eastern equatorial Pacific between 1650 and 1900 C.E. and wetter conditions and frequent El Niño events during the twentieth century.

Acknowledgments

We thank S. Truebe, M. Miller, N. Dozouville, R. Pepolas, D. Ruiz, A. Tudhope, M. Wilson, C. Chilcot, M. Parrales, and J. Suarez for providing assistance in the field and L. Cruz, E. Rosero, and their crews for ship and logistical support. We are grateful to K. Domanik, S. LeRoy, and C. Routson for their help analyzing samples and the Charles Darwin Research Station and the Galápagos National Park for facilitating all aspects of the project. We also thank W. Kenney and M. Brenner for Pb-210 analyses and the University of Arizona and the National Ocean Sciences AMS facilities for radiocarbon measurements. Finally, we thank Ellen Thomas and Emi Ito for their insightful reviews of the manuscript. This research was supported by the National Science Foundation (NSF) RAPID, P2C2, and Atmospheric and Geospace Sciences Paleoclimate Programs (awards AGS-1256970 and AGS- 1561121), the NOAA Climate Program Office, The University of Arizona Department of Geosciences, and the Philanthropic Education Organization. All monitoring data, sediment records, and age models developed here are available at the National Center for Environmental Information (formerly the National Climatic Data Center) paleoclimatology database (https://www.ncdc.noaa.gov/paleo/study/22274).

References

An, S.-I., and J. Choi (2015), Why the twenty-first century tropical Pacific trend pattern cannot significantly influence ENSO amplitude?, *Clim. Dyn.*, *44*(1–2), 133–146, doi:10.1007/s00382-014-2233-2.

Ashok, K., S. K. Behera, S. A. Rao, H. Weng, and T. Yamagata (2007), El Niño Modoki and its possible teleconnection, *J. Geophys. Res.*, *112*, C11007, doi:10.1029/2006JC003798.

American Public Health Association, American Water Works Association, Water Environment Federation (1998), Checking correctness of analyses, in *Standard Methods of Examination of Water and Wastewater*, pp. 1–21, McGraw Hill, Baltimore, Md.

Baguley, T. (2012), *Serious Stats: A Guide to Advanced Statistics for the Behavioral Sciences*, Palgrave Macmillan, London.

Bates, D., M. Mächler, B. Bolker, and S. Walker (2015), Fitting linear mixed-effects models using lme4, *J. Stat. Softw.*, *67*(1), 1–48, doi:10.18637/jss.v067.i01.

Battarbee, R. W., and M. J. Kneen (1982), The use of electronically counted microspheres in absolute diatom analysis, *Limnol. Oceanogr.*, *27*(1), 184–188, doi:10.4319/lo.1982.27.1.0184.

Blaauw, M., and J. A. Christen (2011), Flexible paleoclimate age-depth models using an autoregressive gamma process, *Bayesian Anal.*, *6*(3), 457–474, doi:10.1214/ba/1339616472.

Bony, S., K. M. Lau, and Y. C. Sud (1997), Sea surface temperature and large-scale circulation influences on tropical greenhouse effect and cloud radiative forcing, *J. Clim.*, *10*(8), 2055–2077, doi:10.1175/1520-0442(1997)010<2055:SSTALS>2.0.CO;2.

Charles Darwin Foundation (2012), CDF meteorological database - base de datosmeterologico de la FCD. Online data portal - portal de datos en linea.

Clement, A. C., R. Seager, M. A. Cane, and S. E. Zebiak (1996), An ocean dynamical thermostat, *J. Clim.*, *9*(9), 2190–2196, doi:10.1175/1520-0442(1996)009<2190:AODT>2.0.CO;2.

Clement, A., P. DiNezio, and C. Deser (2011), Rethinking the Ocean's role in the southern oscillation, *J. Clim.*, *24*(15), 4056–4072, doi:10.1175/2011JCLI3973.1.

Cobb, K. M., C. D. Charles, H. Cheng, and R. L. Edwards (2003), El Niño/southern oscillation and tropical Pacific climate during the last millennium, *Nature*, *424*(6946), 271–276, doi:10.1038/nature01779.

Cobb, K. M., N. Westphal, H. R. Sayani, J. T. Watson, E. Di Lorenzo, H. Cheng, R. L. Edwards, and C. D. Charles (2013), Highly variable el Nino-southern oscillation throughout the Holocene, *Science*, *339*(6115), 67–70, doi:10.1126/science.1228246.

Collins, A. F., M. B. Bush, and J. P. Sachs (2013), Microrefugia and species persistence in the Galápagos highlands: A 26,000-year paleoecological perspective, *Front. Genet.*, *4*, 269, doi:10.3389/fgene.2013.00269.

Conroy, J. L., A. Restrepo, J. T. Overpeck, M. Steinitz-Kannan, J. E. Cole, M. B. Bush, and P. A. Colinvaux (2009), Unprecedented recent warming of surface temperatures in the eastern tropical Pacific Ocean, *Nat. Geosci.*, *2*(1), 46–50, doi:10.1038/ngeo390.

Conroy, J. L., D. M. Thompson, A. Collins, J. T. Overpeck, M. B. Bush, and J. E. Cole (2014), Climate influences on water and sediment properties of Genovesa crater Lake, Galápagos, *J. Paleolimnol.*, *52*(4), 331–347, doi:10.1007/s10933-014-9797-z.

Conroy, J. L., J. T. Overpeck, and J. E. Cole (2010), El Niño/Southern Oscillation and changes in the zonal gradient of tropical Pacific sea surface temperature over the last 1.2 ka, *PAGES news*.

Conroy, J. L., J. T. Overpeck, J. E. Cole, T. M. Shanahan, and M. Steinitz-Kannan (2008), Holocene changes in eastern tropical Pacific climate inferred from a Galápagos lake sediment record, *Quat. Sci. Rev.*, *27*(11–12), 1166–1180, doi:10.1016/j.quascirev.2008.02.015.

Corrège, T., T. Delcroix, J. Recy, W. Beck, G. Cabioch, and F. Le Cornec (2000), Evidence for stronger El Niño–Southern Oscillation (ENSO) events in a mid-Holocene massive coral, *Paleoceanography*, *15*(4), 465–470, doi:10.1029/1999PA000409.

Deser, C., A. S. Phillips, and M. A. Alexander (2010a), Twentieth century tropical sea surface temperature trends revisited, *Geophys. Res. Lett.*, *37*, L10701, doi:10.1029/2010GL043321.
Deser, C., A. S. Phillips, and M. A. Alexander (2010b), Twentieth century tropical sea surface temperature trends revisited, *Geophys. Res. Lett.*, *37*, L10701, doi:10.1029/2010GL043321.
DiNezio, P. N., G. A. Vecchi, and A. C. Clement (2013), Detectability of changes in the Walker circulation in response to global warming, *J. Clim.*, *26*(12), 4038–4048, doi:10.1175/JCLI-D-12-00531.1.
Donders, T. H., F. Wagner-Cremer, and H. Visscher (2008), Integration of proxy data and model scenarios for the mid-Holocene onset of modern ENSO variability, *Quat. Sci. Rev.*, *27*(5–6), 571–579, doi:10.1016/j.quascirev.2007.11.010.
Faegri, K., and J. Iversen (1989), *Textbook of Pollen Analysis*, 4th ed., edited by K. Faegri, P. E. Kaland, and K. Krzywinski, John Wiley, New York.
Franz, H. (1980), Old soils and land surfaces on the Galápagos islands, *GeoJournal*, *4*(2), 182–184, doi:10.1007/BF00160745.
Freeze, R., and J. Cherry (1979), *Groundwater*, Prentice-Hall, Englewood Cliffs, N. J.
Gieskes, J. M., and W. C. Rogers (1973), Alkalinity determination in interstitial waters of marine sediments, *J. Sediment. Res.*, *43*(1).
Gruber, A. (1972), Fluctuations in the position of the ITCZ in the Atlantic and Pacific oceans, *J. Atmos. Sci.*, *29*(1), 193–197.
Gu, G., R. F. Adler, A. H. Sobel, G. Gu, R. F. Adler, and A. H. Sobel (2005), The eastern Pacific ITCZ during the boreal spring, *J. Atmos. Sci.*, *62*(4), 1157–1174, doi:10.1175/JAS3402.1.
Guilyardi, E., H. Bellenger, M. Collins, S. Ferrett, and W. Cai (2012), A first look at ENSO in CMIP5, *Clivar Exchanges*, *17*(1), 29–32.
Hamann, O. (1979), On climatic conditions, vegetation types, and leaf size in the Galápagos Islands, *Biotropica*, *11*(2), 101, doi:10.2307/2387785.
Hayes, S. P., A. Sumi, K. Takeuchi, L. J. Mangum, J. Picaut, A. Sumi, and K. Takeuchi (1991), TOGA-TAO: A moored array for real-time measurements in the tropical Pacific Ocean, *Bull. Am. Meteorol. Soc.*, *72*(3), 339–347, doi:10.1175/1520-0477(1991)072<0339:TTAMAF>2.0.CO;2.
Hua, Q., M. Barbetti, and A. Z. Rakowski (2013), Atmospheric radiocarbon for the period 1950–2010, *Radiocarbon*, *55*(4), 2059–2072.
Huang, B., et al. (2015), Extended Reconstructed Sea surface temperature version 4 (ERSST.v4). Part I: Upgrades and Intercomparisons, *J. Clim.*, *28*(3), 911–930, doi:10.1175/JCLI-D-14-00006.1.
Jha, B., Z.-Z. Hu, and A. Kumar (2014), SST and ENSO variability and change simulated in historical experiments of CMIP5 models, *Clim. Dyn.*, *42*(7–8), 2113–2124, doi:10.1007/s00382-013-1803-z.
Johnson, J. W., E. H. Oelkers, and H. C. Helgeson (1992), SUPCRT92: A software package for calculating the standard molal thermodynamic properties of minerals, gases, aqueous species, and reactions from 1 to 5000 bar and 0 to 1000°C, *Comput. Geosci.*, *18*(7), 899–947, doi:10.1016/0098-3004(92)90029-Q.
Jones, B. F., and D. M. Deocampo (2003), *Geochemistry of Saline Lakes*, vol. 5, p. 605, Elsevier, Amsterdam.
Jørgensen, B. B., and Y. Cohen (2003), Solar Lake (Sinai). 5. The sulfur cycle of the bcnthic cyanobacterial mats1, *Limnol. Oceanogr.*, *22*(4), 657–666, doi:10.4319/lo.1977.22.4.0657.
Karamperidou, C., P. N. Di Nezio, A. Timmermann, F.-F. Jin, and K. M. Cobb (2015), The response of ENSO flavors to mid-Holocene climate: Implications for proxy interpretation, *Paleoceanography*, *30*, 527–547, doi:10.1002/2014PA002742.
Karnauskas, K. B., R. Seager, A. Kaplan, Y. Kushnir, and M. A. Cane (2009), Observed strengthening of the Zonal Sea surface temperature gradient across the equatorial Pacific Ocean, *J. Clim.*, *22*(16), 4316–4321, doi:10.1175/2009JCLI2936.1.
Kessler, W. S. (2006), The circulation of the eastern tropical Pacific: A review, *Prog. Oceanogr.*, *69*(2–4), 181–217, doi:10.1016/j.pocean.2006.03.009.
Kim, S. T., and J. Y. Yu (2012), The two types of ENSO in CMIP5 models, *Geophys. Res. Lett.*, *39*, L11704, doi:10.1029/2012GL052006.
Koutavas, A., and S. Joanides (2012), El Niño–southern oscillation extrema in the Holocene and last glacial maximum, *Paleoceanography*, *27*, PA4208, doi:10.1029/2012PA002378.
Koutavas, A., J. Lynch-Stieglitz, T. M. Marchitto, and J. P. Sachs (2002), El Niño-like pattern in ice age tropical Pacific sea surface temperature, *Science*, *297*(5579), 226–230, doi:10.1126/science.1072376.
Koutavas, A., P. B. deMenocal, G. C. Olive, and J. Lynch-Stieglitz (2006), Mid-Holocene el Niño–southern oscillation (ENSO) attenuation revealed by individual foraminifera in eastern tropical Pacific sediments, *Geology*, *34*(12), 993–996, doi:10.1130/G22810A.1.
Liu, Y., L. Xie, J. M. Morrison, and D. Kamykowski (2013), Dynamic downscaling of the impact of climate change on the ocean circulation in the Galápagos archipelago, *Adv. Meteorol.*, *2013*(2), 1–18, doi:10.1155/2013/837432.
Liu, Z., S. Vavrus, F. He, N. Wen, Y. Zhong, S. Vavrus, F. He, N. Wen, and Y. Zhong (2005), Rethinking tropical ocean response to global warming: The enhanced equatorial warming, *J. Clim.*, *18*(22), 4684–4700, doi:10.1175/JCLI3579.1.
Mackenzie, F. T., S. Vink, R. Wollast, and L. Chou (1995), Comparative geochemistry of marine saline lakes, in *Physics and Chemistry of Lakes*, pp. 265–278, Springer, Berlin.
Makou, M. C., T. I. Eglinton, D. W. Oppo, and K. A. Hughen (2010), Postglacial changes in el Nino and la Nina behavior, *Geology*, *38*(1), 43–46, doi:10.1130/G30366.1.
Martín-Puertas, C., B. L. Valero-Garcés, M. P. Mata, A. Moreno, S. Giralt, F. Martínez-Ruiz, and F. Jiménez-Espejo (2011), Geochemical processes in a Mediterranean Lake: A high-resolution study of the last 4,000 years in Zoñar Lake, southern Spain, *J. Paleolimnol.*, *46*(3), 405–421, doi:10.1007/s10933-009-9373-0.
McGregor, H. V. (2004), Western Pacific coral δ^{18}O records of anomalous Holocene variability in the El Niño–Southern Oscillation, *Geophys. Res. Lett.*, *31*, L11204, doi:10.1029/2004GL019972.
McGregor, H. V., M. J. Fischer, M. K. Gagan, D. Fink, S. J. Phipps, H. Wong, and C. D. Woodroffe (2013), A weak El Niño/Southern Oscillation with delayed seasonal growth around 4,300 years ago, *Nat. Geosci.*, *6*(11), 949–953, doi:10.1038/ngeo1936.
McKay, N. P., D. S. Kaufman, and N. Michelutti (2008), Biogenic silica concentration as a high-resolution, quantitative temperature proxy at Hallet Lake, south-central Alaska, *Geophys. Res. Lett.*, *35*, L05709, doi:10.1029/2007GL032876.
McPhaden, M. J. (1993), TOGA-TAO and the 1991–93 El Niño–Southern Oscillation event, *Oceanography*, *6*(2), 36–44.
Mitchell, T. P., T. P. Mitchell, and J. M. Wallace (1992), The annual cycle in equatorial convection and sea surface temperature, *J. Clim.*, *5*(10), 1140–1156, doi:10.1175/1520-0442(1992)005<1140:TACIEC>2.0.CO;2.
Morse, J. W., and F. T. Mackenzie (1990), *Geochemistry of Sedimentary Carbonates*, Elsevier, Amsterdam.
Mortlock, R. A., and P. N. Froelich (1989), A simple method for the rapid determination of biogenic opal in pelagic marine sediments, *Deep Sea Res. Part A*, *36*(9), 1415–1426.
Moy, C. M., G. O. Seltzer, D. T. Rodbell, and D. M. Anderson (2002), Variability of el Niño/southern oscillation activity at millennial timescales during the Holocene epoch, *Nature*, *420*(6912), 162–165, doi:10.1038/nature01194.
Newton, A., R. Thunell, and L. Stott (2006), Climate and hydrographic variability in the indo-Pacific warm pool during the last millennium, *Geophys. Res. Lett.*, *33*, L19710, doi:10.1029/2006GL027234.

Oppo, D. W., Y. Rosenthal, and B. K. Linsley (2009), 2,000-year-long temperature and hydrology reconstructions from the indo-Pacific warm pool, *Nature*, *460*(7259), 1113–1116, doi:10.1038/nature08233.
Parkhurst, D. L., and C. Appelo (2013), Description of input and examples for PHREEQC version 3—A computer program for speciation, batch-reaction, one-dimensional transport, and inverse geochemical calculations, *U.S. Geol. Surv. Techniques Methods*, *6*(A43), 497.
Peixoto, J. P., and A. H. Oort (1992), *Physics of Climate*, Am. Inst. of Phys., New York.
Pryet, A., C. Domínguez, P. F. Tomai, C. Chaumont, N. d'Ozouville, M. Villacís, and S. Violette (2012), Quantification of cloud water interception along the windward slope of Santa Cruz Island, Galápagos (Ecuador), *Agric. For. Meteorol.*, *161*, 94–106, doi:10.1016/j.agrformet.2012.03.018.
R Core Team (2016), R: A language and environment for statistical computing, R Foundation for Statistical Computing, Vienna. [Availalble at http://www.R-project.org/.]
Rasband, W. S. (2004), ImageJ; US National Institutes of Health: Bethesda, Md., 1997-2006,
Reimer, P. J., et al. (2013), IntCal13 and Marine13 radiocarbon age calibration curves 0-50,000 years cal BP, *Radiocarbon*, *55*(4), 1869–1887, doi:10.2458/azu_js_rc.55.16947.
Rein, B., A. Lückge, L. Reinhardt, F. Sirocko, A. Wolf, and W.-C. Dullo (2005), El Niño variability off Peru during the last 20,000 years, *Paleoceanography*, *20*, PA4003, doi:10.1029/2004PA001099.
Restrepo, A., P. Colinvaux, M. Bush, A. Correa-Metrio, J. Conroy, M. R. Gardener, P. Jaramillo, M. Steinitz-Kannan, and J. Overpeck (2012), Impacts of climate variability and human colonization on the vegetation of the Galápagos Islands, *Ecology*, *93*(8), 1853–1866, doi:10.1890/11-1545.1.
Reynolds, R. W., N. A. Rayner, T. M. Smith, D. C. Stokes, and W. Wang (2002), An improved in situ and satellite SST analysis for climate, *J. Clim.*, *15*(13), 1609–1625, doi:10.1175/1520-0442(2002)015<1609:AIISAS>2.0.CO;2.
Riedinger, M. A., M. Steinitz-Kannan, W. M. Last, and M. Brenner (2002), A ~6100 14C yr record of el Niño activity from the Galápagos Islands, *J. Paleolimnol.*, *27*(1), 1–7, doi:10.1023/A:1013514408468.
Sachs, J. P., D. Sachse, R. H. Smittenberg, Z. Zhang, D. S. Battisti, and S. Golubic (2009), Southward movement of the Pacific intertropical convergence zone AD 1400–1850, *Nat. Geosci.*, *2*(7), 519–525, doi:10.1038/ngeo554.
Sandeep, S., F. Stordal, P. D. Sardeshmukh, and G. P. Compo (2014), Pacific Walker circulation variability in coupled and uncoupled climate models, *Clim. Dyn.*, *43*(1–2), 103–117, doi:10.1007/s00382-014-2135-3.
Shanahan, T. M., J. T. Overpeck, W. E. Sharp, C. A. Scholz, and J. A. Arko (2007), Simulating the response of a closed-basin lake to recent climate changes in tropical West Africa (Lake Bosumtwi, Ghana), *Hydrol. Process.*, *21*(13), 1678–1691, doi:10.1002/hyp.6359.
Shuttleworth, W. J. (1993), Evaporation, in *Handbook of Hydrology*, edited by D. R. Maidment, pp. 4–1, McGraw-Hill, New York.
Soil Survey Staff (2010), *Keys to Soil Taxonomy*, 11th ed., USDA-Natural Resources Conservation Service, Washington, D. C.
Solomon, A., and M. Newman (2012), Reconciling disparate twentieth-century indo-Pacific ocean temperature trends in the instrumental record, *Nat. Clim. Chang.*, *2*(9), 691–699, doi:10.1038/nclimate1591.
Stabel, H. H. (1986), Calcite precipitation in Lake Constance: Chemical equilibrium, sedimentation, and nucleation by algae, *Limnol. Oceanogr.*, *31*(5), 1081–1094, doi:10.4319/lo.1986.31.5.1081.
Stocker, T. F., D. Qin, G.-K. Plattner, M. M. B. Tignor, S. K. Allen, J. Boschung, A. Nauels, Y. Xia, V. Bex, and P. M. Midgley (2013), Climate phenomena and their relevance for future regional climate change, in *Climate Change the Physical Science Basis. Contribution of Working Group I to the Fifth Assessment of the Intergovernmental Panel on Climate Change*, edited by T. F. Stocker et al., pp. 1217–1308, Cambridge Univ. Press, Cambridge.
Stott, L., K. Cannariato, R. Thunell, G. H. Haug, A. Koutavas, and S. Lund (2004), Decline of surface temperature and salinity in the western tropical Pacific Ocean in the Holocene epoch, *Nature*, *431*(7004), 56–59, doi:10.1038/nature02903.
Swanson, F. J., H. W. Baitis, J. Lexa, and J. Dymond (1974), Geology of Santiago, Rábida, and Pinzón Islands, Galápagos, *Geol. Soc. Am. Bull.*, *85*(11), 1803, doi:10.1130/0016-7606(1974)85<1803:GOSRAP>2.0.CO;2.
Team, R. C. (2014), *R: A Language and Environment for Statistical Computing*, p. 2013, R Foundation for Statistical Computing, Vienna.
Thompson, D. M., T. R. Ault, M. N. Evans, J. E. Cole, and J. Emile Geay (2011), Comparison of observed and simulated tropical climate trends using a forward model of coral δ 18O, *Geophys. Res. Lett.*, *38*, L14706, doi:10.1029/2011GL048224.
Tierney, J. E., D. W. Oppo, Y. Rosenthal, J. M. Russell, and B. K. Linsley (2010), Coordinated hydrological regimes in the indo-Pacific region during the past two millennia, *Paleoceanography*, *25*, PA1102, doi:10.1029/2009PA001871.
Trueman, M., and N. d'Ozouville (2010), Characterizing the Galápagos terrestrial climate in the face of global climate change, *Galapagos Res.*, *67*, 26–37.
Tudhope, A. W. (2001), Variability in the el Nino-southern oscillation through a glacial-interglacial cycle, *Science*, *291*(5508), 1511–1517, doi:10.1126/science.1057969.
Vecchi, G. A., A. Clement, and B. J. Soden (2008), Examining the tropical Pacific's response to global warming, *Eos Trans. AGU*, *89*(9), 81–83, doi:10.1029/2008EO090002.
Waliser, D. E., and C. Gautier (1993), A satellite-derived climatology of the ITCZ, *J. Clim.*, *6*(11), 2162–2174, doi:10.1175/1520-0442(1993)006<2162:ASDCOT>2.0.CO;2.
Wang, C., and P. C. Fiedler (2006), ENSO variability and the eastern tropical Pacific: A review, *Prog. Oceanogr.*, *69*(2–4), 239–266, doi:10.1016/j.pocean.2006.03.004.
Watanabe, M., J.-S. Kug, F.-F. Jin, M. Collins, M. Ohba, and A. T. Wittenberg (2012), Uncertainty in the ENSO amplitude change from the past to the future, *Geophys. Res. Lett.*, *39*, L20703, doi:10.1029/2012GL053305.
Weare, B. C., A. R. Navato, R. E. Newell, B. C. Weare, A. R. Navato, and R. E. Newell (1976), Empirical orthogonal analysis of Pacific sea surface temperatures, *J. Phys. Oceanogr.*, *6*(5), 671–678, doi:10.1175/1520-0485(1976)006<0671:EOAOPS>2.0.CO;2.
Weng, H., K. Ashok, S. K. Behera, S. A. Rao, and T. Yamagata (2007), Impacts of recent El Niño Modoki on dry/wet conditions in the Pacific rim during boreal summer, *Clim. Dyn.*, *29*(2–3), 113–129, doi:10.1007/s00382-007-0234-0.
Wolff, M. (2010), Galápagos does not show recent warming but increased seasonality, *Galapagos Res.*, *67*, 38–44.
Wyrtki, K. (1981), An estimate of equatorial upwelling in the Pacific, *J. Phys. Oceanogr.*, *11*(9), 1205–1214, doi:10.1175/1520-0485(1981)011<1205:AEOEUI>2.0.CO;2.
Yan, H., L. Sun, Y. Wang, W. Huang, S. Qiu, and C. Yang (2011), A record of the Southern Oscillation Index for the past 2,000 years from precipitation proxies, *Nat. Geosci.*, *4*(9), 611–614, doi:10.1038/ngeo1231.
Yeh, S.-W., Y.-G. Ham, and J.-Y. Lee (2012), Changes in the Tropical Pacific SST trend from CMIP3 to CMIP5 and its implication of ENSO, *J. Clim.*, *25*(21), 7764–7771, doi:10.1175/JCLI-D-12-00304.1.
Zimmerman, D. W., and B. D. Zumbo (1993), Relative power of the Wilcoxon test, the Friedman test, and repeated-measures ANOVA on ranks, *J. Exp. Educ.*, *62*(1), 75–86, doi:10.1080/00220973.1993.9943832.